Heft R597 (2021)

FVV-Informationstagung Turbomaschinen | Frühjahrstagung 2021 – Frankfurt (Digitalkonferenz)

Simulation-Rissverhalten-Grobkorn

FVV Nr. 1251 | Abschlussbericht (AB)

1 | Materialprüfungsanstalt (MPA), Universität Stuttgart
Prof. Dr.-Ing. Stefan Weihe

2 | Institut für Werkstoffkunde (IfW), Technische Universität Darmstadt
Prof. Dr.-Ing. Matthias Oechsner

Thema:	Simulation des Rissverhaltens von grobkörnigen Nickelgusslegierungen bei hohen Temperaturen
Laufzeit:	01.11.2016 – 31.10.2020
Fördergeber:	Bundesministerium für Wirtschaft und Energie / Arbeitsgemeinschaft industrieller Forschungsvereinigungen e.V. (BMWi/AiF)
Fördernummer(n):	IGF 19226 N
Vorsitzende(r) projekt-begleitender Ausschuss:	Dipl.-Ing. Markus Fried (MTU Aero Engines AG)
Bearbeiter und Verfasser:	Dr.-Ing. Magdalena Speicher (MPA) Dr. rer. nat. Christopher Kohler (MPA) Lorenz Wöllmann, M.Sc. (IfW) Dr.-Ing. Falk Müller (IfW) Dr.-Ing. Christian Kontermann (IfW)
Vortragende(r):	Lorenz Wöllmann, M.Sc. (IfW)

Danksagung

Dieser Bericht ist das wissenschaftliche Ergebnis einer Forschungsaufgabe, die von der Forschungsvereinigung Verbrennungskraftmaschinen (FVV) e. V. gestellt und an der Materialprüfungsanstalt (MPA) der Universität Stuttgart unter der Leitung von Prof. Dr.-Ing. Stefan Weihe sowie am Institut für Werkstoffkunde (IfW) der Technischen Universität Darmstadt unter der Leitung von Prof. Dr.-Ing. Matthias Oechsner bearbeitet wurde.

Die FVV dankt den Professoren Weihe und Oechsner und den wissenschaftlichen Bearbeitern Dr.-Ing. Magdalena Speicher (MPA), Dr. rer. nat. Christopher Kohler (MPA), M.Sc. Lorenz Wöllmann (IfW), Dr.-Ing. Falk Müller (IfW) und Dr.-Ing. Christian Kontermann (IfW) für die Durchführung des Vorhabens sowie der Arbeitsgemeinschaft industrieller Forschungsvereinigungen (AiF) e. V. für die finanzielle Förderung. Das Vorhaben wurde von einem Arbeitskreis der FVV unter der Leitung von Herrn Dipl.-Ing. Markus Fried (MTU Aero Engines AG) begleitet. Diesem projektbegleitenden Ausschuss gebührt unser Dank für die große Unterstützung.

Das Forschungsvorhaben wurde im Rahmen des Programms zur Förderung der industriellen Gemeinschaftsforschung (IGF-Nr. 19226 N) vom Bundesministerium für Wirtschaft und Energie (BMWi) über die Arbeitsgemeinschaft industrieller Forschungsvereinigungen (AiF) e. V. aufgrund eines Beschlusses des Deutschen Bundestages gefördert.

Gefördert durch:
Bundesministerium für Wirtschaft und Energie
aufgrund eines Beschlusses des Deutschen Bundestages
Forschungsnetzwerk Mittelstand
Industrielle Gemeinschaftsforschung
Forschungsvereinigung Verbrennungskraftmaschinen

Kurzfassung

Bei der Bewertung der Zuverlässigkeit und Lebensdauer von Hochtemperaturbauteilen ist die Vorhersage des Anriss- und Risswachstumsverhaltens von außerordentlicher Bedeutung. Bei Bauteilen aus grobkörnigen Nickelgusslegierungen, wie beispielsweise Turbinenschaufeln von stationären Gasturbinen und Flugzeugturbinen, ist die bisherige Vorgehensweise zur Bewertung der Zuverlässigkeit und Lebensdauer sehr konservativ. Ein besseres Verständnis zum Einfluss grobkörniger Gussgefüge auf die Eigenschaften kann dazu beitragen, eine präzisere und weniger konservative Bewertung zu ermöglichen und adäquate Werkzeuge, die den lokalen Spannungszustand und somit das im Einsatz zu beobachtende Rissinitiierungs- und -wachstumsverhalten berücksichtigen, zu schaffen.

Das Ziel des im vorliegenden Schlussbericht zusammengefassten Forschungsvorhabens war es, den Einfluss der Kornstruktur auf das Hochtemperaturrissverhalten unter Kriech(ermüdungs)beanspruchung in grobkörnigen Nickelgusslegierungen mit praxisrelevanten Korndurchmessern größer 2 mm zu untersuchen und zu beschreiben. Die Untersuchungen wurden dabei am Polykristall IN713 CC und an der einkristallinen Variante IN713 SC schwerpunktmäßig bei 850 °C durchgeführt. Unterschiedliche orientierte Einkristalle wurden untersucht, um entsprechende Modellierungsansätze mit den passenden Werkstoffdaten zu hinterlegen. Die Beschreibungen zum Kriech(ermüdungs)rissverhalten basierten auf der Analyse der unstetigen Rissausbreitung (Rissstopp, Rissumlenkung, Inselbildung, Anrissbildung usw. abhängig vom lokalen Gefügezustand) unter der Verwendung von Ansätzen, die die Kornstruktur berücksichtigen können.

Im vorliegenden Bericht werden die experimentellen und numerischen Ergebnisse des Projekts vorgestellt. Die Phänomene Verformung, Rissbildung und Risswachstum wurden hierbei auf der mikrostrukturellen Ebene (Korn) untersucht, im Gegensatz zu bisherigen Ansätzen, die den (feinkristallinen) Polykristall als Kontinuum annehmen. Ein wesentlicher Aspekt hierbei war die Identifizierung kritischer Parameter für die Rissinitiierung durch Kombination der Ergebnisse aus Kriech(ermüdungs)rissversuchen, metallographischen und kristallographischen Untersuchungen und unter Verwendung eines anisotropen linear-elastischen Verformungsmodells sowie zeitabhängiger Beschreibungsansätze.

Anhand der Korrelation von Mikrostrukturgrößen und aufgetretenen Rissen wurden Korngröße und Korngrenzenlänge als geometrische Parameter sowie Orientierungsunterschiede und Schmidfaktoren für verschiedene Gleitsysteme untersucht. Mit Hilfe des elastischen und des kristallplastischen (Cailletaud) Modells hat sich aufgrund des Verformungsverhaltens die Kombination der Kornorientierung im Bereich von [025] und [101] als kritisch ergeben und die Umgebung der Körner mit diesen Orientierungen fungieren als möglicher Ort der Rissinitiierung unter Kriechbelastung.

Zur Validierung der Modelle und der kritischen Parameter wurden Kriechversuche an flachen Proben mit begleitender optischer Dehnfeldmessung durchgeführt. Die mit dem kristallplastischen Modell berechnete Kriechdehnung zeigt eine gute Übereinstimmung mit der optischen Messung. Mögliche Abweichungen resultieren aus der getroffenen Annahme, dass sich die Kornstruktur in Tiefenrichtung gleichmäßig fortsetzt. Weiterhin wird der Anteil der primären Kriechdehnung von dem kristallplastischen Ansatz aktuell etwas unterschätzt. In einem Validierungsversuch wird die als kritisch identifizierte Orientierungskombination zwischen [025] und [101] bestätigt, jedoch sind für eine finale Bestimmung eines kritischen Parameters weitere Forschungsarbeiten notwendig.

Issue R597 (2021)

FVV Information Sessions Turbomachinery | Spring 2021 – Frankfurt (Digital Conference)

Simulation-Crack Behaviour-Coarse Grain

FVV no. 1251 | Final report (AB)

1 | Materials Testing Institute (MPA), University of Stuttgart
Prof. Dr.-Ing. Stefan Weihe

2 | Institute for Materials Technology (IfW), Technical University of Darmstadt
Prof. Dr.-Ing. Matthias Oechsner

Full title:	Simulation of crack behaviour of nickel cast alloys with large grain size at high temperature
Duration:	01.11.2016 – 31.10.2020
Funding organisation(s):	Federal Ministry for Economic Affairs and Energy / German Federation of Industrial Research Associations eV (BMWi/AiF)
Funding number(s):	IGF 19226 N
Project user committee chair:	Dipl.-Ing. Markus Fried (MTU Aero Engines AG)
Research associate(s) / author(s):	Dr.-Ing. Magdalena Speicher (MPA) Dr. rer. nat. Christopher Kohler (MPA) Lorenz Wöllmann, M.Sc. (IfW) Dr.-Ing. Falk Müller (IfW) Dr.-Ing. Christian Kontermann (IfW)
Lecturer(s):	Lorenz Wöllmann, M.Sc. (IfW)

Acknowledgement

This report is the scientific result of a research project undertaken by the FVV (The Research Association for Combustion Engines e.V.) and performed by the Materials Testing Institute at the University of Stuttgart (MPA) under the direction of Prof. Dr.-Ing. Stefan Weihe, and by the Institute for Materials Technology (IfW) at Technical University of Darmstadt under the direction of Prof. Dr.-Ing. Matthias Oechsner.

The FVV would like to thank the professors Weihe and Oechsner and their respective scientific research assistants – Dr.-Ing. Magdalena Speicher (MPA), Dr. rer. nat. Christopher Kohler (MPA), M. Sc. Lorenz Wöllmann (IfW), Dr.-Ing. Falk Müller (IfW) and Dr.-Ing. Christian Kontermann (IfW) – for the implementation of the project. Special thanks are due to the AiF (German Federation of Industrial Research Associations eV) for funding the project. The project was conducted by an expert group led by Dipl.-Ing. Markus Fried (MTU Aero Engines AG). We gratefully acknowledge the support received from the chairman and from all members of the project user committee.

The research project was carried out in the framework of the industrial collective research programme (IGF no. 19226 N). It was supported by the Federal Ministry for Economic Affairs and Energy (BMWi) through the AiF (German Federation of Industrial Research Associations eV) based on a decision taken by the German Bundestag.

Supported by:

Federal Ministry for Economic Affairs and Energy

on the basis of a decision by the German Bundestag

Forschungsnetzwerk Mittelstand

Industrielle Gemeinschaftsforschung

FVV Research Association for Combustion Engines

Abstract

The prediction of the crack initiation and crack growth behaviour when determining the reliability and lifetime of high-temperature components is of major importance. For parts made of coarse-grained cast nickel alloys, e.g. turbine blades of stationary gas turbines and aircraft engines, the current procedure for assessing reliability and service life is very conservative. A better understanding of the effect of coarse-grained cast microstructures on their properties can help to enable a more precise and less conservative assessment and to create adequate tools that take into account the local stress state, and thus the crack initiation and growth behaviour observed in use.

The objective of this research project was the investigation and description of the effects of the grain structure on the high-temperature crack behaviour under creep (fatigue) loading in coarse-grained nickel cast alloy IN713 with practice-oriented grain diameters greater than 2 mm. The examinations were performed on polycrystalline IN713 CC and the single crystalline type IN713 SC mainly at 850 °C. Different single crystal orientations were examined to provide proper material data for corresponding modelling approaches. The descriptions of creep (fatigue) crack behaviour are based on the analysis of the discontinuous crack propagation (crack arrest, crack deflection, formation of crack-free areas, crack initiation etc. depending on the local microstructure) using approaches that take the grain structure into account.

This report presents the experimental and numerical results of this project. The phenomena of deformation, crack formation and crack growth were investigated on the microstructural level (grain), unlike previous approaches, which assume the (finely crystalline) polycrystal as a continuum. A crucial aspect considered here was the identification of critical parameters for crack initiation by combining the findings from creep (fatigue) testing, metallographic and crystallographic examinations, and using the anisotropic linear-elastic deformation model as well as time-dependent description approaches.

Based on the correlation of microstructure and occurring cracks, grain size and grain boundary length were analysed as geometric parameters, as well as differences in orientation and Schmid factors for different slip systems. Using the elastic and the crystal plasticity (Cailletaud) model, the combination of grain orientation in the range of [025] and [101] was found to be critical for the crack formation due to the deformation behaviour, and the areas around the grains with these orientations act as a possible crack initiation site under creep loading.

For the validation of the models and the critical parameters, creep tests with accompanying optical strain field measurements were carried out on flat specimens. The calculated creep strain from the crystal plasticity model shows good agreement with the optical measurement. Possible deviations result in particular from the assumption that the grain structure continues uniformly in the depth direction. Furthermore, the primary creep strain is slightly underestimated by the crystal plasticity approach. In a validation test, the critical orientation combination between [025] and [101] has been verified. However, further research is needed to identify a final “critical parameter” determining creep crack initiation.

1 Introduction

Nickel-based alloys have a special significance due to their excellent mechanical high temperature characteristics in combination with a high corrosion resistance. They are used for the mechanically and thermally high-loaded parts in the design of turbines, engines and reactors [Pol06].

Cast nickel alloys with a coarse-grained microstructure are applied in turbines and combustion chambers, which are subject to creep (fatigue) loading during operation. The grain morphology in cast parts depends mainly on cooling rates during solidification resulting in typically rather fine grains in thin-walled regions of the parts (e.g. airfoils) and rather coarse grains in thick-walled cross sections (e.g. blade root). The grain structure (grain size, grain morphology, grain boundaries and grain aspect ratio) thereby affects the strength, deformation and damage behaviour. Furthermore, the grain size has an influence on the mechanical properties under high-temperature loading so that grain sizes of several millimetres may improve creep resistance. However, the grain boundaries itself may serve as starting point for intergranular creep cracks.

Generally, such nickel-based alloys can be manufactured as conventionally cast (CC), directionally solidified (DS) and single-crystalline solidified (SC) types. For DS and SC types, the increased resistance against creep damage is based on the targeted orientation and/or elimination of grain boundaries.

In order to optimize the use, and thus maximizing the application potential of the materials and ensuring their safe operation, it is necessary to better understand and describe the crack initiation and crack growth behaviour of such coarse-grained nickel cast alloys. In previous research projects [Ber10, Oec14, Oec17], the formation and growth of cracks, initiated just by the grain orientations at the grain boundaries and triple points, in some isothermal and anisothermal creep (fatigue) crack growth experiments was observed. In such cases, the crack behaviour is characterized by an inhomogeneous crack front as well as crack arrest and crack deflection effects. The influence of the grain structure on the crack behaviour under creep (fatigue) loading in materials with a coarse-grained microstructure is of major importance, but currently insufficiently investigated and understood. Therefore, in this work the influence of the grain structure and local grain orientations were examined and correlated with the crack behaviour. The aim was to identify critical crystallographic orientations and/or orientation relationships as well as critical grain morphology and grain boundary parameters that determine the crack initiation behaviour under creep (fatigue) loading.

2 Theoretical Background

The knowledge about the crack initiation and crack growth behaviour is essential when assessing the component lifetime and determining maintenance intervals. Aside from fatigue loading, the time and temperature with respect to creep (and oxidation) play a crucial role in operation. If these factors are not taken into account, there will be a significant overestimation of the remaining lifetime. The fatigue crack behaviour was and still is extensively examined using nickel cast alloys. In contrast, the creep crack behaviour of nickel cast alloys has only been insufficiently researched so far, especially for grain sizes larger than 2 mm [Bra95, Naz83, Sha89, Bot97, Sun13].

In the projects FVV 746 (AiF 12308N) [Ber03] and FVV 884 (AiF 14609N) [Ber08], the creep crack behaviour of the coarse-grained cast nickel alloy IN-738 LC was investigated using compact tension

and corner-crack specimens at 700 °C and 850 °C. Partially, in these examples the grain size was even larger than 5 mm. As previously mentioned, during testing discontinuous crack growth could be observed characterized by an inhomogeneous crack front with crack arrest and crack deflection effects (Figure 2-1a). In [Cor04], similar phenomena were observed at the coarse-grained nickel cast alloy 625 with grain sizes up to even 50 mm. This phenomenon has been concluded under both creep and creep-fatigue loading. Investigations at the polycrystalline alloy M-247 CC HIP in [Oec14] showed that crack initiation and crack growth can occur in specimens with short initial crack starter notches even outside the manufactured notch (Figure 2-1b). In the projects FVV 959 (AiF 15525N) [Oec11] and FVV 1145 (AiF 17809N) [Oec17], similar phenomena were also observed under thermo-mechanical fatigue (TMF) loading. So far, this behaviour was only described sporadically in literature. Nevertheless, the grain orientation itself was identified as a possible factor to influence the crack initiation and crack growth and consequently the lifetime of a real component.

a) b)

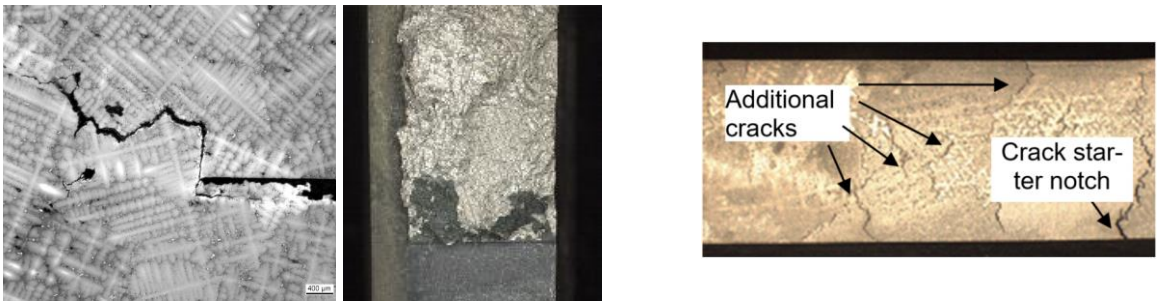

Figure 2-1: Crack growth a) in the polycrystalline, coarse-grained alloy IN738LC under creep loading [Ber03]; b) Forming of additional cracks in corner-crack specimens of M-247 CC HIP under creep and creep-fatigue loading [Oec14].

In a polycrystalline material, the orientation-dependent properties of an individual grain averaged over a high number of grains lead to a quasi-isotropic material behaviour. For technical components or specimens with a coarse-grained structure, this assumption is no longer valid if only a small number of grains is present, especially for materials with high anisotropy, resulting in a strongly different local behaviour. Even macroscopic homogeneous loads lead to local strain and stress concentrations, which can contribute to creep crack formation. The elastic anisotropy for a face-centred cubic (fcc) lattice for instance is described via three independent elastic constants. This results in the direction dependence of the engineering constants Young's modulus *E*, shear modulus *G* and Poisson ratio ν for every single grain as it is described for example in [Sie01]. Under external loading, compatibility stresses arise because free deformation is prevented at the interface (Figure 2-2).

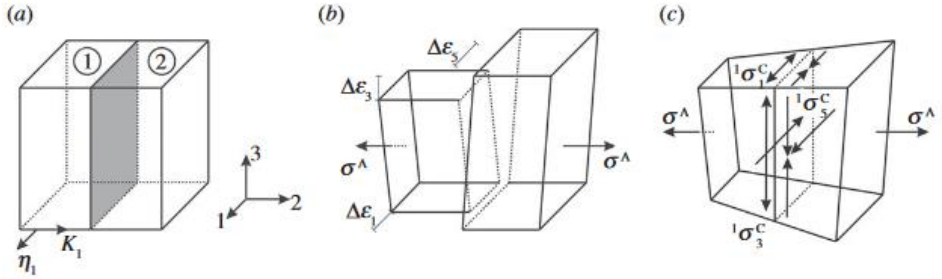

Figure 2-2: Compatibility stresses at a grain boundary under external loading [Pfe17].

The occurring stress concentrations due to elastic anisotropy are reported as a cause for transcrystalline and intercrystalline crack formation under fatigue loading in austenitic steel [Hei90], copper bicrystals [Per94] and nickel cast alloys [Eng18]. Since stress concentrations depend on geometrical aspects of each individual grain and its position in relation to other grains, anisotropic elastic microstructure models were used to calculate strain distributions to get an indication for a crack initiation site [Kru02, Kno05]. Theoretical approaches based on the orientation-dependent Young's modulus *E* and the Schmid factor *m* are applied. An "*E*·*m* model" was developed which estimates the resulting shear stress depending on the orientation and the Schmid factor with existing homogeneous strain. When this shear stress is exceeded, it results in a fatigue crack initiation [Eng18].

Under creep loading, different mechanisms are relevant and crack initiation and growth take place at grain boundaries mostly perpendicular to the loading direction. Based on the crystallographic characterization, the orientation difference of two grains can be described by the misorientation angle. For bicrystal specimens of the nickel cast alloys René N4 and GTD 444, in [Sti15] creep properties were investigated as a function of misorientation angle and compared to the creep behaviour of single crystals. For René N4, the creep rupture life significantly decreases with a higher misorientation angle and the creep elongation dropped for misorientation angles larger than 20°. The specimens failed during the secondary creep regime with low rupture ductility. In contrast, the creep rupture lives of GTD 444 were independent of misorientation and rupture occurred within the tertiary regime [Sti15].

Creep rupture tests were carried out in [Kno01, Mac82, Sas96] to describe the plastically anisotropic properties of nickel-based single crystals. For MAR-M247, creep tests were performed at 774 °C and a high stress of 724 MPa. Compared with creep tests on MAR-M200 at 760 °C for both materials, extremely poor creep properties were reported for [011] orientations. The longest creep rupture lives were identified for [111] and [001] orientations (Figure 2-3). The creep rupture lives differ between 1 h and 1200 h due to strong differences of active mechanisms in the primary creep regime. In order to estimate the orientation-dependent creep behaviour, the Schmid factor provides information regarding which grain orientation is favourable for slip. During first stage creep, the {111}<112> slip system is active and transition to secondary creep can only happen if sufficient strain hardening occurs due to multiple slip. For secondary creep, the octahedral slip system {111}<101> becomes active. Also, single crystal rotation during plastic deformation is reported [Mac82].

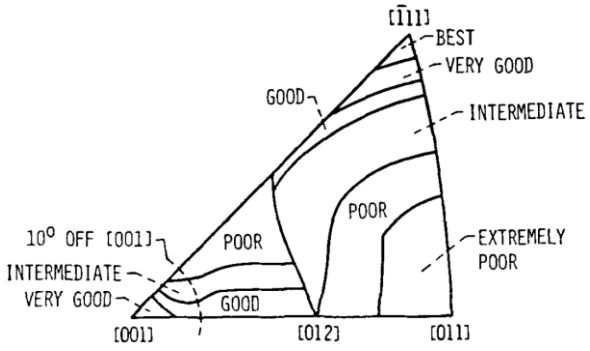

Figure 2-3: Orientation dependence of the stress rupture lives for MAR-M247 and MAR-M200 single crystals at 760 °C and 774 °C [Mac82].

For creep rupture tests on CMSX-4 single crystals at 850 °C as well as lower stresses of 500 MPa and 600 MPa, the same sensitivity of primary creep, especially for [001] and [011] orientations, were identified. Single slip orientations like [011] or [256] show high primary creep rates and short creep rupture times. In contrast to MAR-M247, [111] oriented specimens of CMSX-4 showed a poor creep resistance. However, the creep resistance was evaluated by reaching 0.5% and 2% strain lifetime, thus the primary and secondary creep regime was investigated in this study. These strain lifetimes mainly depend on primary creep, which act strongly anisotropic at 850 °C [Sas96]. The Schmid factor of the most highly stressed slip system for octahedral and {111}<112> is shown in Figure 2-4. The activity of different slip systems depends on loading conditions and temperature, but it was noted that "*to fully address single crystal deformation between 1023 and 1223 K therefore it is proposed that one must consider the activity of both the <112>{111} and the <011>{111} type slip systems*" [Kno01].

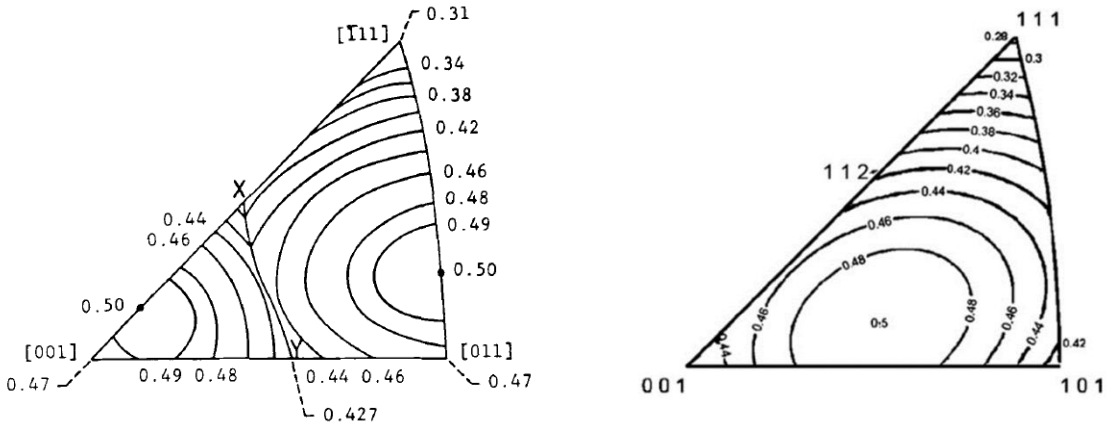

Figure 2-4: Orientation dependence of the Schmid factor for the most highly stressed {111}<112> (left) or {111}<101> (right) slip system.

A third slip system, which is known as cubic slip system {001}<110>, is reported in literature. Whereas experiments show that macroscopic cubic slip occurs quite exceptionally, this system is required to model realistic creep rates for [111] orientations [Kno01, Tin10]. However, there are also contradictory study results. For creep tests on single crystals of the nickel cast alloy SRR 99 at 850 °C and different stress levels, cubic slip was identified as dominant for orientations from [112] – [111] based on observations of changes in the specimen's cross-sectional shape during creep deformation [Pan97]. Due to the ambiguous mechanisms of the direction-dependent plastic deformation in single crystals, the transfer to single grains of a polycrystalline material is not trivial.

Since the reasons for the crack behaviour outlined above are still insufficiently investigated and understood, the conservatism in component design is high to ensure life within the prescribed inspection intervals. With a better knowledge about crack initiation and propagation in connection with microstructural parameters, reliable methods for the assessment of such components can be developed, and thus conservatism can be reduced. Therefore, numerical tools are to be used to get a better understanding about these phenomena and to qualify and quantify them.

In order to model the deformation behaviour and the crack initiation processes in polycrystalline materials at the grain level, computational crystal plasticity, together with finite element (FE) microstructure models, is a suitable modelling technique and has been widely used [Har99, Lin10]. In crystal plasticity,

the macroscopic stress is locally resolved onto the slip systems by using Schmid's law as well as the local shear strain rate for each slip system and is computed as a function of the resolved shear stress. This can be done by using phenomenological constitutive laws for the slip systems or by using the physical mechanisms of dislocation glide. The total viscoplastic strain rate is obtained as a sum of the contributions of all slip systems. For the modelling of polycrystalline materials, microstructure models have been used e.g. by constructing representative volume elements with random orientations of cubic grains [Ben03] or of grains obtained by Voronoi tessellations [She08]. Furthermore, models have been obtained through reconstruction of the surface microstructure from scans gained via electron backscatter diffraction (EBSD) [Che07]. For the fatigue crack initiation, several criteria have already been adopted. In [Gui10], a stress-based criterion was applied, which uses the maximum resolved shear stress on the slip systems. A strain-based criterion was developed in [Dun07] using the effective accumulated plastic strain. In [Che07], the local plastic energy dissipation was used to predict the initiation of fatigue cracks. However, as mentioned before, the reliable criteria for the assessment of creep (fatigue) cracks considering the grain structure and grain properties are still missing and have to be established.

3 Research Objectives and Scientific Approach

Since the influence of the grain structure on the crack behaviour under creep and creep-fatigue loading in coarse-grained materials is insufficiently understood at present, this research project deals with the investigation and description of the effects of the grain structure on the high temperature crack behaviour in coarse-grained nickel cast alloy IN713 with grain diameters larger than 2 mm. As mentioned in chapter 2, experience from application field and from laboratory experiments in previous research projects show that the crack behaviour of high-temperature components made of nickel cast materials is significantly influenced by the grain structure itself. Hence, the grain orientation is assumed to be an essential parameter based on the fcc lattice structure and the resulting anisotropy of the material. The spatial arrangement of large grains with local anisotropic deformation and damage behaviour leads to local stress concentrations even at a macroscopic homogeneous loading. These stress concentration spots can lead to crack initiation and crack growth. Therefore, the size, morphology and position of neighbouring grains must be considered as a further influencing factor on the crack behaviour.

The basic tasks of the research project were:

- the investigation and description of the crack behaviour of coarse-grained nickel cast alloys in relation to crack initiation and crack propagation by considering the local stresses and strains on the microstructural level (grain),
- the determination and implementation of the anisotropy of the material and the simulation of deformation and damage behaviour,
- the identification of the critical factors influencing the crack behaviour under creep (fatigue) loading.

For the successful implementation of the project, it was essential to select a test material that could be cast both polycrystalline with a sufficiently coarse grain as well as single-crystalline. Single-crystal versions of the alloy were required to determine the anisotropic material behaviour. In coordination with the

industrial partners within the W14 working group, nickel cast alloy IN713 was chosen, which is used in gas turbines and the turbo charger sector.

Grain size, grain boundary morphology and orientation correlations between neighbouring grains were examined as fundamental parameters aside from the local grain orientation. In order to identify critical parameters, experimental examinations were performed on polycrystalline alloy IN713 CC at 850 °C regarding creep and creep-fatigue crack behaviour, and occurring phenomena are subsequently characterized metallographically and crystallographically.

The findings gained through experiments were used for theoretical problem descriptions. This includes an anisotropic linear-elastic, an anisotropic Chaboche and a crystal plasticity model. The necessary material parameters were determined on single-crystalline IN713 SC with different crystallographic orientations. For this purpose, the resonance frequencies were measured to determine the elastic constants and tensile, complex LCF as well as creep rupture tests were carried out. Aside from determining the model parameters, an automated process was developed for a simplified transfer of the measured real-based grain structure from an EBSD map into an FE model. The objective of the simulation was to identify critical parameters and to synchronize them with the experiments. Finally, validation tests were carried out, which were accompanied by strain field measurements using a stereo camera system to quantify locally occurring strains and relate them to the grain structure. Thus, a comparison between the experiment and the simulation lead to a first verification of the material models and assessment approaches. In this way, the identification of critical factors which influence the crack behaviour under creep (fatigue) loading of coarse-grained materials was performed.

4 Material characterization

For the experimental investigations within this project, nickel cast alloy IN713 was chosen due to the aforementioned reasons. The raw material was provided by MTU Aero Engines AG in hot isostatically pressed (HIP) and precipitation hardened condition. Subsequently, the chemical composition was checked via optical emission spectroscopy (OES) (Table 4-1).

Table 4-1: Chemical composition of nickel cast alloy IN713 determined by optical emission spectroscopy (OES).

Element	***C***	***Si***	***Mn***	***Al***	***B***	***Co***	***Cr***	***Mo***	***Nb + Ta***	***Ti***	***Ni***
	wt.% (from OES)										
Conventionally Cast (CC)	0.10	0.054	<0.01	5.81	0.013	0.17	12.93	3.96	2.20	1.00	73.40
Single Crystal (SC)	0.123	0.063	<0.01	5.75	0.013	0.736	13.23	3.55	2.00	1.01	72.26

The chemical composition of the melt fulfils the specification [AMS14]. The conventionally cast test material was delivered as bars with a diameter of 31 mm. The single-crystalline material was provided as bars with a diameter of 21 mm and slabs with the dimensions of 120 mm x 100 mm x 24 mm with a [001]-casting direction.

The grain structure was documented with etched longitudinal and cross sections from various test bars. As an example, macro images of sections from test bar 655-1 are shown in Figure 4-1. Here, the influence of the cooling rate during solidification can be seen resulting in different grain size and shape distribution. In the outer area, the cast bars show significantly smaller grain sizes than in the centre due to faster cooling rates. An average grain size was measured by the intercept technique in an area of 10 x 10 mm in the cross sections and an area of 10 mm width in the longitudinal sections as these correspond approximately to the specimen dimensions. The average grain size was determined to be 6 mm for the cross sections and 3 mm for the longitudinal sections.

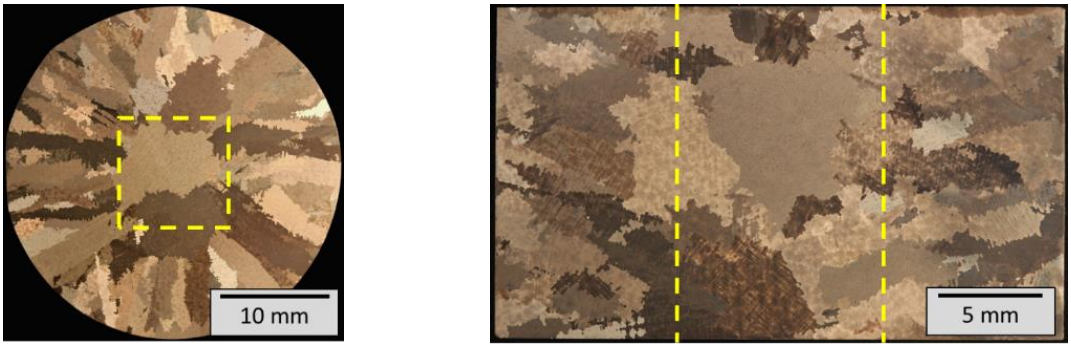

Figure 4-1: Macro images of the etched sections for grain size determination from test bar 655-1 of IN713, left: Cross section, right: Longitudinal section.

The macro images of two single crystals with different orientations show regular patterns on the surfaces of the transverse sections, Figure 4-2. These patterns show the dendritic structure resulting from the solidification process. During the solidification, the primary dendrites grow along the longitudinal direction (pull-off direction) of the test bar. The secondary dendrite arms lead to a cruciform pattern for the [001]-oriented single crystal bar. Another cross section was made from the thread of a [121]-oriented specimen. The angle between the [121]-direction and the [001] growing direction of the dendrites is about 35°. Therefore, the secondary dendrite arms appear tilted in the transverse section.

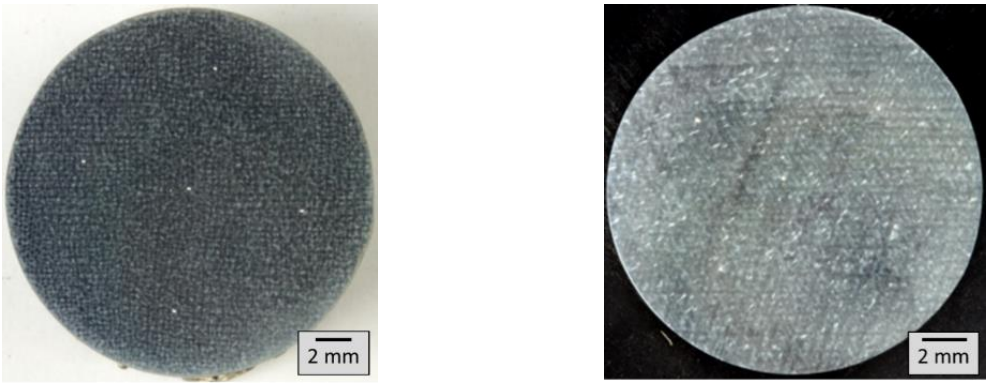

Figure 4-2: Macro images of the single crystalline material IN713, left: [001]-orientation, right: [121]-orientation.

The microstructure of the conventionally cast and single crystalline test material was characterized by scanning electron microscopy (SEM). The microstructure of all alloys consists of γ-matrix, γ'-precipitates, primary carbides of the MC-type (Ti, Nb, Mo) and secondary $M_{23}C_6$ carbides (rich in Cr and Mo), Figure 4-3.

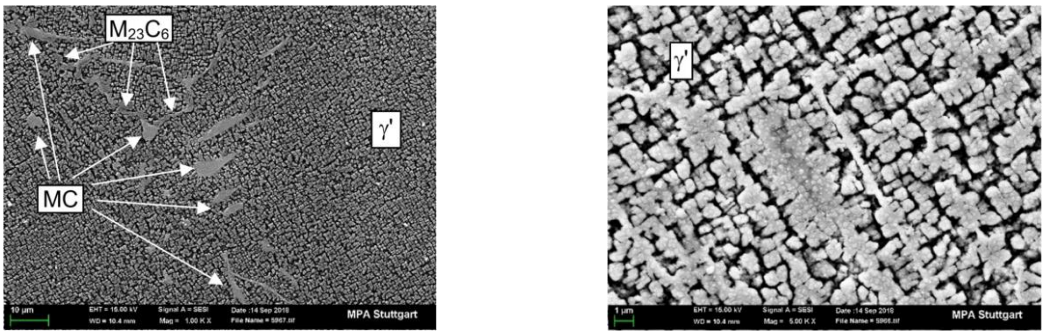

Figure 4-3: SEM images of IN713 CC; left: Carbides and γ'-phase; right: γ'-phase.

5 Anisotropic material properties

When describing anisotropic material properties, a distinction must be made between elastic and inelastic behaviour. The elastic behaviour can be described under the assumption of cubic symmetry (fcc) with three independent entries of the stiffness matrix C_{11}, C_{12} and C_{44}. These temperature dependent parameters are called elastic constants. The determination of them was done by resonant ultrasound spectroscopy, which was developed for cubic specimens by Demarest [Dem71] and subsequently extended for rods with rectangular cross sections [Ohn76].

5.1 Resonance frequency measurement

For the measurement of the elastic constants at elevated temperature, the change in specimen dimensions and density due to thermal expansion was measured on a cylindrical specimen with a push-road dilatometer according to DIN 51 045-1 (2005). The measurement was performed dynamically with a heating rate of 3 K/min in the temperature range from room temperature (RT) to 900 °C under helium as protective gas. In the present cubic symmetry, the thermal expansion acts isotropically. Therefore, it is sufficient to determine the thermal expansion for one orientation. The measurement was carried out at the Austrian Foundry Research Institut (ÖGI - Österreichisches Gießerei-Institut) on two <100>-oriented, single-crystalline samples and the mean value was determined. The resonant frequencies of three single crystalline specimens with known, different orientations were identified at 24 °C and 850 °C and the elastic constants were calculated as a solution of an inverse problem (Table 5-1). The natural frequencies of the specimens calculated with the finite element method were iteratively adjusted to the measured resonance frequencies. Kindly, these measurements were performed at the Bundesanstalt für Materialforschung und -prüfung (BAM) at the division Experimental and Model Based Mechanical Behaviour of Materials.

Table 5-1: Measured elastic constants and Zener (anisotropy) ratio of IN713 at 24 °C and 850 °C.

IN713	T = 24 °C	T = 850 °C
C_{11} (GPa)	247	203
C_{12} (GPa)	162	142
C_{44} (GPa)	129	100
A_{Zener}	3.04	3.28

The determined elastic constants are consistent with the values found in literature. A detailed overview for different nickel-based alloys in a temperature range from RT up to 1200 °C can be found in [Li15].

At 850 °C, the Zener anisotropy ratio is given between 2.7 and 3.4. So the measured value for IN713 lies in the upper range which indicates a strong elastic anisotropy.

5.2 Elastic anisotropy

The orientation dependence of the elastic material properties *E* (Young's modulus) and ν (Poisson ratio) resulting from measured elastic constants is described in the following. The Young's modulus varies at 850 °C for the orientations of [001], [101] and [111] between 94 GPa, 160 GPa and 243 GPa (Figure 5-1). Compared to the results of hot tensile tests at 850 °C on [001] and [101]-oriented single crystals, the results differ by +/- 10 GPa.

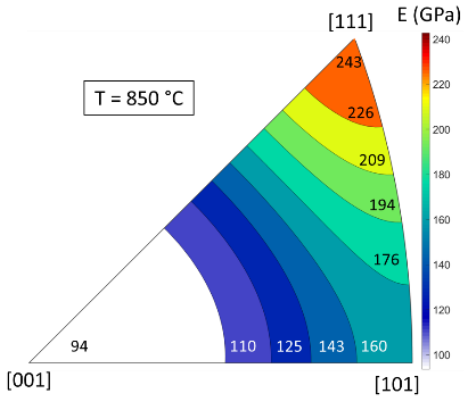

Figure 5-1: Orientation-dependent distribution of the Young's modulus at 850 °C for single crystalline IN713.

The representation of the anisotropic Poisson ratio ν is complex due to its dependence on two directions in contrast to the Young's modulus. For some orientations (in loading direction), the value of ν differs for the transverse directions. The maximum (blue) and minimum (green for > 0 and red for < 0) values of the Poisson ratio can be presented in polar plots projected on different planes with regard to the loading direction. For <100> directions, ν is independent of the transverse direction due to the rotational symmetry and has a value of about 0.4. With a rotation of 45° in the (001) plane to a direction of [110], the Poisson ratio varies between 0.8 for the secondary direction of [001] and -0.15 for the [101] direction. A negative Poisson ratio must be interpreted in such a way that the specimen expands in the corresponding longitudinal direction during tensile load. For [111] or [121] orientations, the variation of the Poisson ratio can be presented by a projection on the (10-1) plane (Figure 5-2).

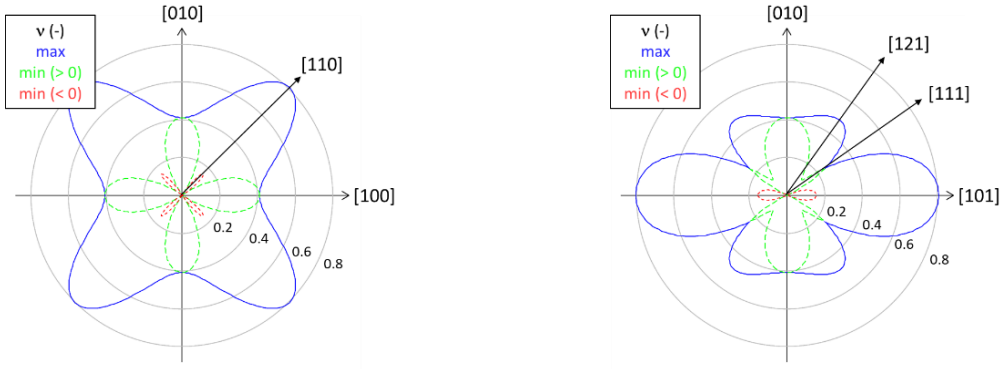

Figure 5-2: Orientation dependence of the Poisson ratio ν at 850 °C for single crystalline IN713, left: Projection on (001)-plane, right: Projection on the (10-1)-plane.

5.3 Creep anisotropy

In order to model the anisotropic viscoplastic behaviour of IN713, a crystal plasticity constitutive law in the form of the Cailletaud model was used [Mer91-1, Mer91-2]. This model consists of single one-dimensional Chaboche models on each slip system.

In crystal plasticity, the inelastic strain rate $\dot{\boldsymbol{\varepsilon}}$ is given as a sum over shear strain rates $\dot{\gamma}^{\alpha}$ on all slip systems α,

$$\dot{\boldsymbol{\varepsilon}} = \sum_{\alpha} \dot{\gamma}^{\alpha}\, \boldsymbol{s}^{\alpha} \otimes \boldsymbol{m}^{\alpha}$$

where $\boldsymbol{m}^{\alpha}$ is the glide plane normal and $\boldsymbol{s}^{\alpha}$ is the slip direction of slip system α. For IN713 with its fcc lattice, 18 slip systems were taken into account: 12 octahedral and 6 cubic slip systems.

The flow condition for each slip system α is

$$f^{\alpha} = |\tau^{\alpha} - X^{\alpha}| - R^{\alpha} - \tau_0^{\alpha} > 0$$

where $\tau^{\alpha} = \boldsymbol{m}^{\alpha} \cdot \boldsymbol{\sigma} \cdot \boldsymbol{s}^{\alpha}$ is the Schmid stress, X^{α} is the kinematic hardening, R^{α} is the isotropic hardening and τ_0^{α} is the initial flow stress. The plastic shear strain rate $\dot{\gamma}^{\alpha}$ is given by

$$\dot{\gamma}^{\alpha} = \dot{p}^{\alpha} \operatorname{sign}(\tau^{\alpha} - X^{\alpha})$$

where $p^{\alpha} = \int |\dot{\gamma}^{\alpha}|\, \mathrm{d}t$ is the accumulated viscoplastic strain.

The time evolution equations for p^{α}, X^{α} and R^{α} are

$$\dot{p}^{\alpha} = \left\langle \frac{|\tau^{\alpha} - X^{\alpha}| - R^{\alpha} - \tau_0^{\alpha}}{K^{\alpha}} \right\rangle^{n^{\alpha}},$$

$$\dot{X}^{\alpha} = C^{\alpha} \varphi(p^{\alpha}) \dot{\gamma}^{\alpha} - D^{\alpha} \dot{p}^{\alpha} X^{\alpha},$$

$$\varphi(p^{\alpha}) = \phi^{\alpha} + (1 - \phi^{\alpha}) e^{-\delta^{\alpha} p^{\alpha}},$$

$$R^{\alpha} = \sum_{\beta=1}^{n} H_{\alpha\beta} Q^{\beta} \left(1 - e^{-b^{\beta} p^{\beta}}\right).$$

Here, K^{α}, n^{α}, τ_0^{α}, C^{α}, D^{α}, ϕ^{α}, δ^{α}, Q^{α}, b^{α} and $H_{\alpha\beta}$ are material parameters.

The Cailletaud model was implemented as an ABAQUS user subroutine using a fully implicit formulation.

The identification of the material parameters using results from experimental tests proceeds as follows: For an initial set of parameters, the Cailletaud model is integrated for a homogeneous system with the same loading history as in the experiment. The difference between the experimental data and the computed data is assessed using a merit function being the mean square deviation. Then, the parameters are iteratively modified and the model is integrated until the merit function reaches a minimum.

In order to identify the material parameters, tensile tests, complex low cycle fatigue tests and creep rupture tests of single crystalline IN713 at 850 °C with different crystal orientations in the loading direction have been conducted. For this purpose, the parameters for creep and fatigue behaviour have been identified separately. In the following, only the identification of the material parameters for creep is described. Using results from creep rupture tests for two stress levels and for two different crystal orientations in loading direction, the optimal material parameters found are listed in Table 5-2.

Table 5-2: Material parameters of the Cailletaud model for creep simulations. The subscripts o and c denote the octahedral and cubic slip system families, respectively. Units are chosen such that time is given in seconds and stress in MPa.

K_o	n_o	C_o	D_o	φ_o	δ_o
7289.55	3.7275	268368	3511.55	0.7621	714.633
K_c	n_c	C_c	D_c	φ_c	δ_c
643.6113	10.8434	1298.77	$8.4638 \cdot 10^{-4}$	10.0	197.151

All parameters not given in Table 5-2 are zero except for the parameters $H_{\alpha\beta}$, which are taken from [Mer91-1, Mer91-2].

The comparison of the experimental creep curves and the calculated creep curves is shown in Figure 5-3.

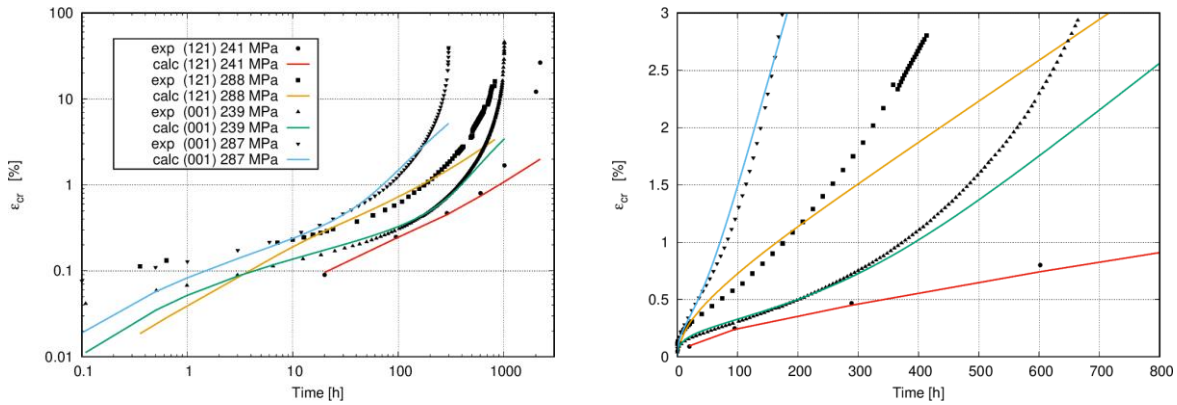

Figure 5-3: Experimental creep curves (symbols) and calculated creep curves (lines) for single crystals, left: Complete creep curves in logarithmic scale, right: Enlargement of the beginning in linear scale.

It should be noted that by using the Cailletaud model in the given form, tertiary creep is not taken into account.

Using the material parameters given in Table 5-2, one can analyse the creep anisotropy resulting from the Cailletaud model. For a given crystal orientation, the creep strain depends on the applied stress and the creep time. For a creep stress of 250 MPa, the creep strain for selected orientations is shown in Figure 5-4 (left).

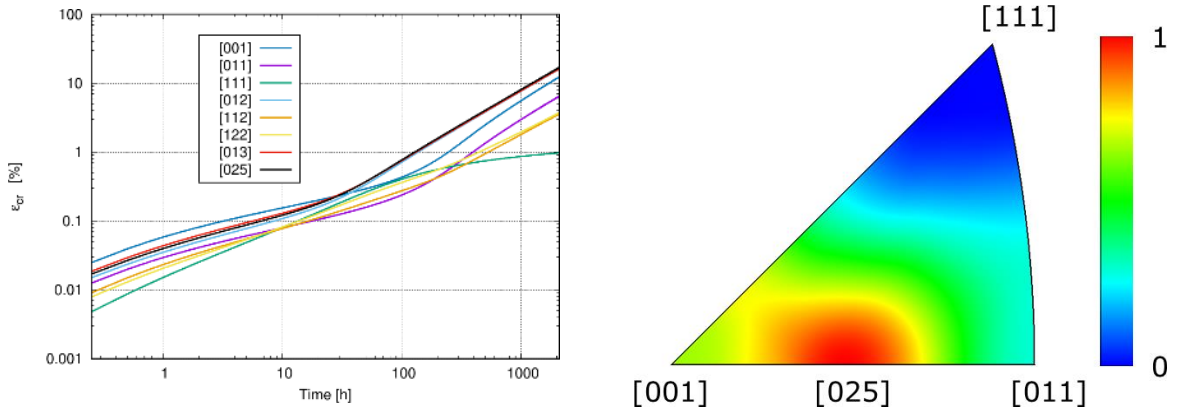

Figure 5-4: Creep curves calculated with the Cailletaud model at 250 MPa with selected crystal orientations in loading direction (left), Relative creep strains for all orientations (right). The applied stress is 250 MPa and the time is 1,000 h.

It can be seen that for short creep times, the [111] direction exhibits the smallest creep strain and the [001] direction the largest one. However, for larger creep times, i.e. for secondary creep, the creep strain is minimum for the [111] direction while the largest creep strain is found in directions close to [025]. In order to better understand the anisotropic creep behaviour, the relative creep strain at the creep time of 1,000 h is plotted for all orientations colour-coded into the standard orientation triangle in Figure 5-4 (right).

Creep simulations at other stress levels indicate that the orientation dependence shown in Figure 5-4 (right) represents a general characteristic of the creep strain dependence for secondary creep: The creep strain is largest for orientations close to the [025] direction and smallest for orientations close to [111].

The simulation of the creep strains for single crystals can be used for a fast estimation of the creep strains in the grains of polycrystalline aggregates by computing the creep strain of each grain separately.

6 Determination of critical parameters for crack initiation

6.1 Procedure

In order to investigate the influence of the grain structure and orientation on the crack behaviour, eight crack growth tests under creep and creep-fatigue loading at 850 °C were carried out. For creep-fatigue loading, long holding times in tension (18 min) led to creep dominated crack growth. As a suitable test geometry, the corner-crack specimen was chosen (Figure 6-1).

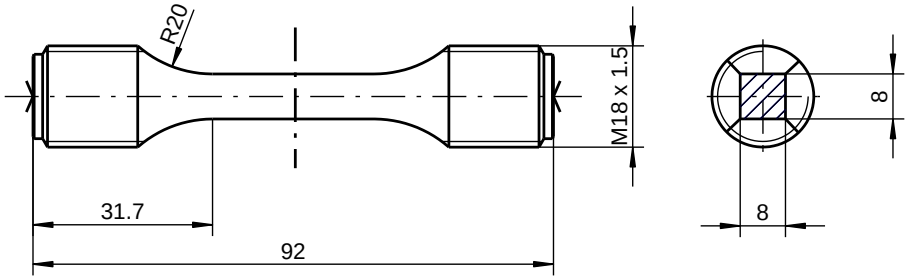

Figure 6-1: Corner-crack specimen geometry for crack growth tests under creep and creep-fatigue loading.

First, the specimen surface or their counterpart from specimen manufacturing via EDM (electrical discharge machining) was examined via electron backscatter diffraction to crystallographically characterise the microstructure. The advantage of scanning the counterpart is the availability of the undamaged microstructure and the smaller size for SEM investigations. However, due to removal of material using the electrical discharge machining (EDM) process for specimen manufacturing, certain differences may occur in the microstructure between specimen surface and its counterpart.

Various approaches were chosen to identify critical grain orientations or grain constellations. After the crack growth test had been carried out, the crack paths were documented on the polished and etched specimen surfaces by optical microscopy. From the EBSD data, microstructure FE models were created [Wol19] according to the developed procedure presented in Figure 6-2.

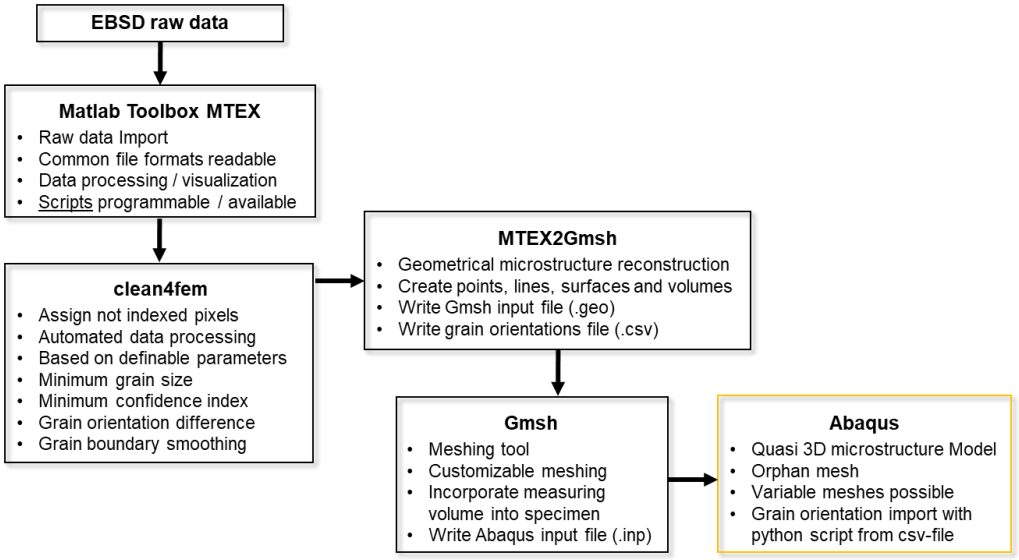

Figure 6-2: Process from EBSD raw data to a microstructure FE model in Abaqus.

The raw data processing was done using the Matlab® toolbox MTex [Bac11]. Based on the clean4fem script [Lat16], a procedure was developed to prepare the microstructural data for further processing. Non-indexed pixels from the EBSD measurement were filled based on the neighbouring orientations and the grain structure was calculated based on high-angle boundaries with at least 15°. Small grains with a size of less than 20 pixels were removed and the grain boundaries were smoothed. The scripts were further developed as part of a bachelor's thesis [Kir18]. Then, a geometrical model of the grain structure was created [Dep19] and meshed in Gmsh. Finally, a quasi 3D microstructure model with a DS-like grain structure was created and embedded in an isotropic environment to apply the boundary conditions (Figure 6-3).

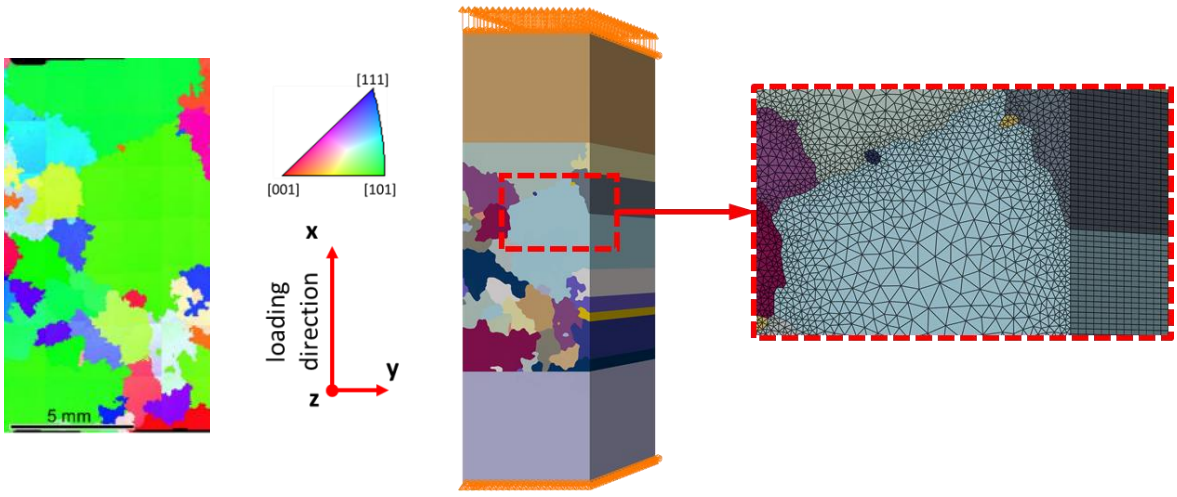

Figure 6-3: From EBSD raw data (x-direction) to the meshed FE model.

The anisotropic linear-elastic model was used to identify local stress and/or strain concentrations that could be responsible for crack initiation. Crystal plasticity simulations were performed with the Cailletaud model to study the creep behaviour of the microstructure models. Afterwards, the local creep strain distributions were analysed to predict the location of creep crack initiation.

6.2 Determination of critical parameters

The described procedure was applied to all crack growth tests with secondary cracks to identify critical parameters based on the microstructure and local stress concentrations from FE models. In the following, two specimens were selected and will be presented as examples.

Correlation of secondary crack path and microstructure

The first specimen from a creep crack growth (CCG) test was chosen due to the clearly visible secondary crack on one side of the corner-crack specimen (Figure 6-4). The CCG-test was carried out at 850 °C with a load of 11.5 kN, which corresponds to a net stress of 185 MPa, and was stopped after 4,582 h due to the increasing load line displacement and potential drop signal. At the crack starter notch, no significant crack growth could be detected.

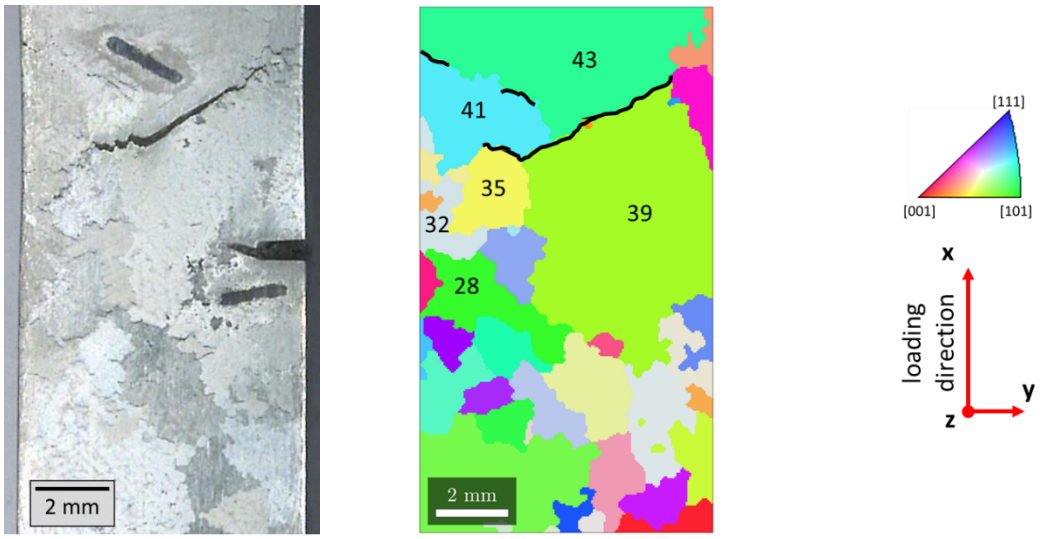

Figure 6-4: Etched surface of the first creep crack growth specimen (left) and the associated EBSD measurement in loading direction (x) (right).

The geometrical parameters, like grain area, grain boundary length and angle to horizontal direction of the cracked grain boundaries, were examined on the specimen surface (Table 6-1). The clearly visible secondary crack between the grains with the ID 39 and 41/43 shows an angle of about 27° to horizontal direction. From experience, the cracks would be expected to propagate at grain boundaries orientated perpendicular to the loading direction. The other secondary cracks in this specimen also lie at a similar angle. The smooth crack edges could indicate the mechanism of grain boundary sliding to be active. Additionally, the involved grains 39, 41 and 43 are large compared to all other visible grains and the common grain boundaries have a summed length of 4.7 mm. Long grain boundaries with an angle of 45° are preferred for grain boundary sliding due to the maximum shear stress [Sou08]. These observations lead to the interim conclusion that a large grain size and a long common grain boundary with an angle of 30° (or more) may be critical for the formation of cracks. Since the crack initiation site cannot be identified because the sample is not visible during the test, all cracked grain boundaries are considered equally critical.

Table 6-1: Geometrical parameters of cracked grain boundaries (GB) referring to Figure 6-4.

Cracked GB (Grain ID's)	Grain area (mm^2)	GB length (mm)	GB angle to horizontal (°)
35 / 41	3.8 / 7.0	1.2	28
39 / 41	28.9 / 7.0	0.9	27
39 / 43	28.9 / 18.0	3.8	27
41 / 43	7.0 / 18.0	3.8	33

Elastic properties of individual grains

In the next step, the orientations of the individual grains were determined from the EBSD measurement and the direction-dependent Young's moduli and Poisson ratios were calculated (Table 6-2). These elastic properties could lead to an incompatibility at grain boundaries due to strong anisotropic behaviour [Pfe17]. From differences in Young's moduli and Poisson ratios, local stress concentrations arise. However, the influence of elastic incompatibility stresses on crack initiation in creep processes is not completely clear so far. For fatigue loading, elastic anisotropy stresses have been identified as a reason for intercrystalline crack initiation [Kru02]. Therefore, critical parameters from FE models with elastic behaviour were subsequently compared with models where (visco)-plasticity is active. Beside considering linear elasticity only, creep processes could lead to stress relaxations at the grain boundaries so that crack initiation might be additionally dependent on plastic anisotropy.

Table 6-2: Grain orientations of selected grains (Figure 6-4), direction-dependent Young's moduli and Poisson ratios.

Grain ID	Orientation [uvw](hkl)	E_x (GPa)	E_y (GPa)	E_z (GPa)	ν_{xy}	ν_{xz}
28	[10 -11 0](0 0 1)	168	168	86	-0.14	0.80
32	[-10 6 3](4 3 7)	160	180	166	0.30	0.37
35	[6 -12 1](1 0 6)	128	134	91	0.14	0.60
39	[-10 7 0](4 6 9)	152	233	187	0.26	0.42
41	[8 -7 3](2 5 6)	193	235	183	0.19	0.42
43	[12 2 -11](11 2 12)	173	91	172	0.77	-0.13

For the microstructure of the examined specimen, the difference of Young's modulus in all three directions of grain 35 and 41 is very large and could be critical for crack initiation. An unusually negative Poisson ratio, meaning that a grain expands in transverse direction under loading, was found for grain 28 and 43. Additionally, a very strong contraction in the perpendicular direction follows. No crack was found at grain boundaries of grain 28, but the large grain 43 shows cracked grain boundaries to grain 39 and 41. Especially the deformation of grain 43 acts contrary to the one of the adjacent grains 39 and 41.

Orientation dependence of critical grain combinations

Looking at the orientations of the involved grains (39, 41, 43), it is clear that it is not sufficient to consider the orientation in loading direction as shown on the EBSD map in Figure 6-4. In order to visualize the

grain orientation with respect to the specimen directions, inverse pole figures (IPF) are suitable. The grain orientation is plotted as the stereographic projection of the crystal direction parallel to the loading direction (Figure 6-5) or the horizontal direction (Figure 6-6). The grains are coloured with the standard IPF colour key for the fcc lattice. Two grains with cracked boundaries during the CCG test are connected by a red line, the black dotted line shows uncracked boundaries.

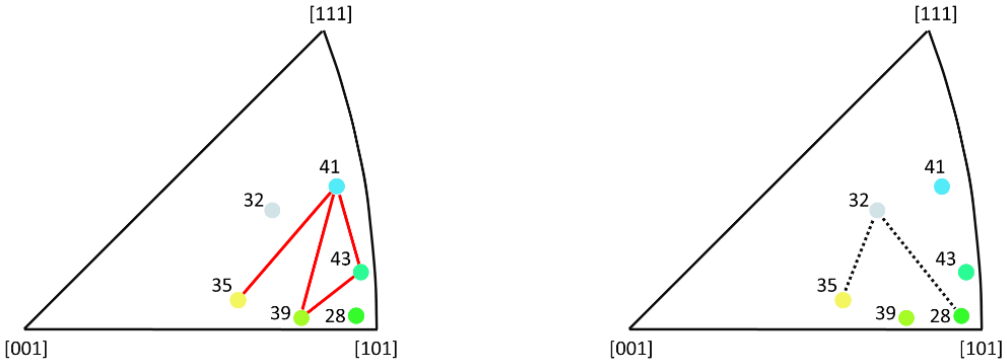

Figure 6-5: Selected grain orientations in loading direction (x) in the inverse pole figure; left: Grains with cracked grain boundaries (red line), right: Grains with uncracked grain boundaries (black dotted line).

Related to the orientation in loading direction, the critical grain boundaries show no significant orientation difference as could be expected. The involved grain orientations are located in the vicinity of the [101] orientation. However, it can be seen that the differences to the uncracked grain combinations are small. The large orientation difference in horizontal direction between the three previously mentioned grains 43 and 39/41 (Figure 6-6) is of major importance. In contrast, the uncracked grain boundaries show a completely different orientation relation.

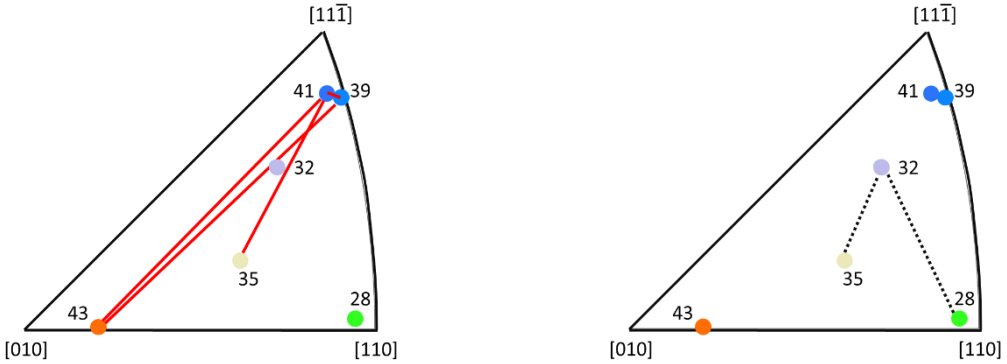

Figure 6-6: Selected grain orientations in horizontal direction (y) in the inverse pole figure; left: Grains with cracked grain boundaries (red line), right: Grains with uncracked grain boundaries (black dotted line).

Grain boundary misorientation and prediction of creep behaviour based on Schmid factors

In order to quantify the orientation difference of two grains by a single parameter, the misorientation angle is used. It is defined as the rotation angle of one axis which is common to both lattices to bring both crystals into alignment. It should be noted that the misorientation does not fully describe the geometry of a grain boundary. Nevertheless, the misorientation could be a critical parameter for crack initiation by describing the strength of the barrier effect of the grain boundary for dislocation transmission on slip systems [Kru02, Sti15]. For the discussed creep crack growth specimen, the misorientation angles between two grains with a cracked grain boundary are between 40° and 45°, the maximum possible angle

is 60° due to the crystal symmetry. Hence, the misorientation as single parameter shows no clear correlation to cracked grain boundaries. Combined with Schmid factor values as estimation of plastic deformation, a prediction for critical grain boundaries may be possible. According to literature, primary creep occurs preferably on {111}<112> slip systems rather than on the typical octahedral fcc slip systems {111}<101>, which are crucial for secondary creep deformation [Mac82]. Thus, the maximum Schmid factors for these slip systems were determined (Table 6-3).

Table 6-3: Comparison of grain combinations of cracked and uncracked grain boundaries with misorientation angles and Schmid factors for the relevant slip systems.

Grain boundary (Grain ID's)	Crack	Misorientation angle (°)	Max. Schmid factor {111}<112>	Max. Schmid factor {111}<101>
28 | 32	No	40.7	0.479 | 0.470	0.433 | 0.475
32 | 35	No	55.8	0.470 | 0.442	0.475 | 0.497
35 | 41	Yes	40.5	0.442 | 0.484	0.497 | 0.439
39 | 41	Yes	40.2	0.465 | 0.484	0.471 | 0.439
39 | 43	Yes	45.8	0.465 | 0.497	0.471 | 0.442
41 | 43	Yes	44.1	0.484 | 0.497	0.439 | 0.442

The highest maximum Schmid factor for primary creep is found in grain 43 with a value of 0.497, which is close to the theoretical maximum of 0.5. The consequences are high primary creep strains in this grain, which extends almost across the entire specimen width. The largest difference in the maximum Schmid factor between two grains resulting in local stress concentrations was found at the grain boundary between grain 35 and 41. Large differences in Schmid factors were reported to be critical for grain boundary cracking [Swa13]. For the octahedral slip systems, it can be concluded that the grain boundary between grain 35 and 41 with the highest maximum Schmid factor and the largest difference is critical for cracking. This is in agreement with the result that the grain boundary of grain 35 and 41 is assumed to be critical for cracking due to their different elastic properties.

Stress distribution from the anisotropic linear-elastic model

In addition, elastic FE calculations were used to verify the hypothesis of induced localized stress concentrations. For this first, the local stress distribution was calculated with the introduced anisotropic elastic model. Figure 6-7 shows the distribution of the von Mises stress and Figure 6-8 the stress in loading direction as well as perpendicular to the loading direction. The maximum stress concentration occurs in the lower area between grain 8 and 11, but no correlation with the detected cracks on the specimen surface can be found due to the vertical alignment of the boundary. A further spot of high stresses arises at the grain boundary between grain 11 and 13 where also no cracks have been found.

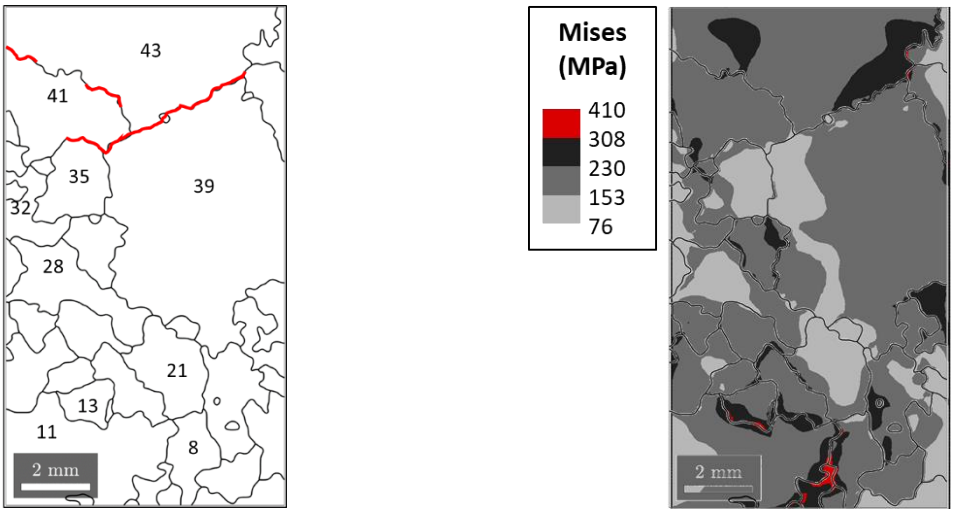

Figure 6-7: Grain structure with cracked grain boundaries (left), Distribution of von Mises stress from the anisotropic linear-elastic model, red: 75-100% of max stress value (right).

In the upper part of the specimen, in grain 43, there are some areas of high stress which correlates with visible creep damage. Nevertheless, no critical parameter can be derived from the von Mises stress distribution in terms of crack formation. The conclusion is the same for the stress distribution in loading and transverse direction. The high stress in grain 43 is remarkable due to the maximum Schmid factor of 0.497 for the primary creep slip system and the correlation of the near [101] orientation with the lowest creep rupture life reported in chapter 2. However, in grain 35, for which a high secondary creep strain is predicted from the high maximum Schmid factor of the octahedral system, only small stresses occur.

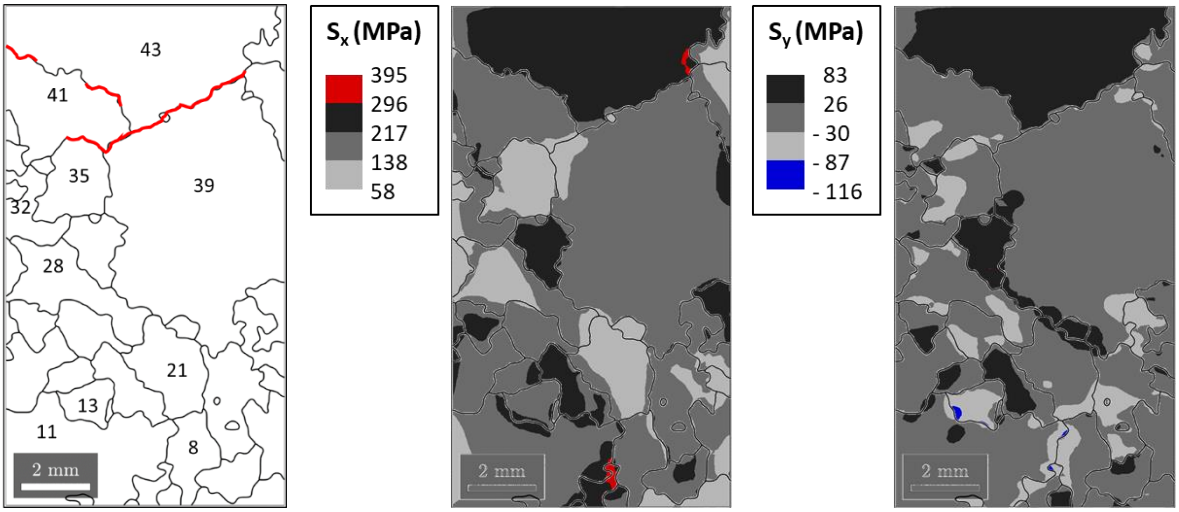

Figure 6-8: Grain structure with cracked grain boundaries (left), Distribution of stresses from the anisotropic linear-elastic model in load direction (x) and perpendicular to load direction (y), red, blue: 75% of max/min stress value as critical parameter (right).

Thus, the determination of a critical parameter just based on stress concentrations itself calculated from the linear-elastic model was not possible. However, there is a certain potential to combine the presented results with the previously proposed parameters concerning orientation differences and Schmid factors.

Calculated creep strain distribution from the Cailletaud model

Beside the elastic simulation, the same FE model was used within a creep simulation applying the Cailletaud model. In Figure 6-9 (right), the distribution of the creep strain in loading direction is shown for a simulation with an external loading of 185 MPa after 3,000 h of creep.

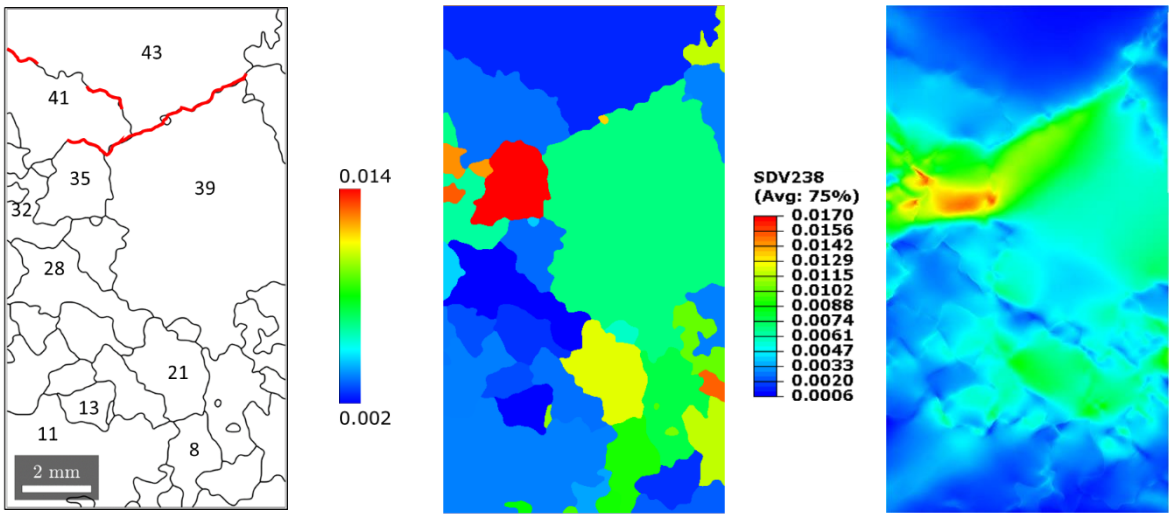

Figure 6-9: Grain structure with cracked grain boundaries (left), creep strain estimation (middle), creep strain in loading direction after 3,000 h creep at 185 MPa simulated with the Cailletaud model (right).

A pronounced creep strain maximum can be identified in grain 35 and smaller maxima in the neighbouring grains. The distribution of creep strain can also be predicted by a creep strain estimation (Figure 6-9 (middle)) using the crystal orientation of the grains and creep simulations for the corresponding single crystals, see chapter 5.3. Indeed, grain 35 has an unfavourable orientation close to the [025] direction. This correlation of grain orientations with creep strain maxima was also found in simulations of other specimens and simulations of model systems with prescribed grain orientations. Furthermore, the correlation of the occurrence of creep strain maxima and secondary cracks (Figure 6-9 (left and right)) was also observed in creep (fatigue) simulations of other specimens investigated. Thus, the initiation of secondary cracks might be connected with the occurrence of large creep strains in unfavourably oriented grains (close to [025]).

Based on the observations, it should be mentioned that different parameters could be critical for creep crack initiation. The creep simulations lead to one grain orientation for which large creep strains were predicted but primary creep on {111}<112> is not considered. In addition, the effect of primary creep and its significance for crack initiation as well as the impact of elastic stress concentrations to creep damage has also not been fully understood until now.

Prediction of creep (fatigue) behaviour based on maximum Schmid factors

Further observations of another specimen support the previous findings. After the creep-fatigue test on the second specimen, a secondary crack on the opposite side of the crack starter notch could be seen. As the EBSD measurement was performed after the test on the damaged specimen's surface, large plastic deformations could be identified within some grains. Three grains are located beside the cracked grain boundary (Figure 6-10).

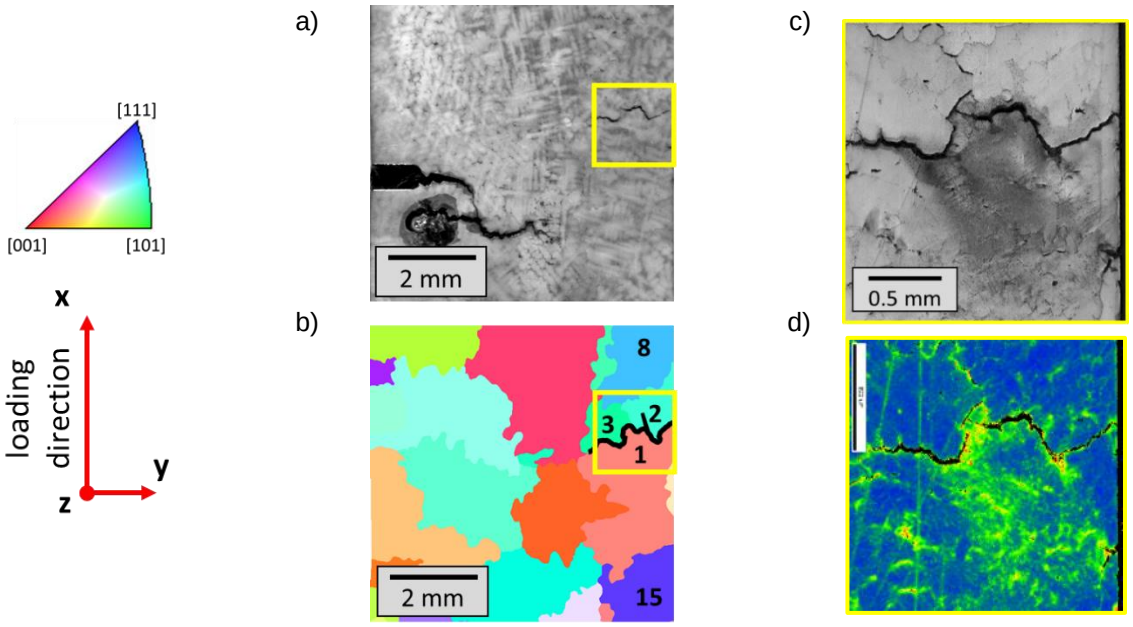

Figure 6-10: Creep-fatigue specimen; a) etched specimen surface, b) EBSD measurement in loading direction, c) Image quality (IQ) map, Kernel average misorientation (KAM) map.

Using the image quality (IQ) map and the Kernel average misorientation (KAM) map, large strains could be detected only in grain 1 with an orientation of [72-1] in loading direction. This orientation roughly coincides with the found critical orientation [025]. Grain 2 and 3 show no evidence of significant plastic deformation but have an orientation of nearly [101], which is characterized by low creep rupture life and strong elastic anisotropy. The grain combination found indicates some similarities to the specimen discussed before (Figure 6-11).

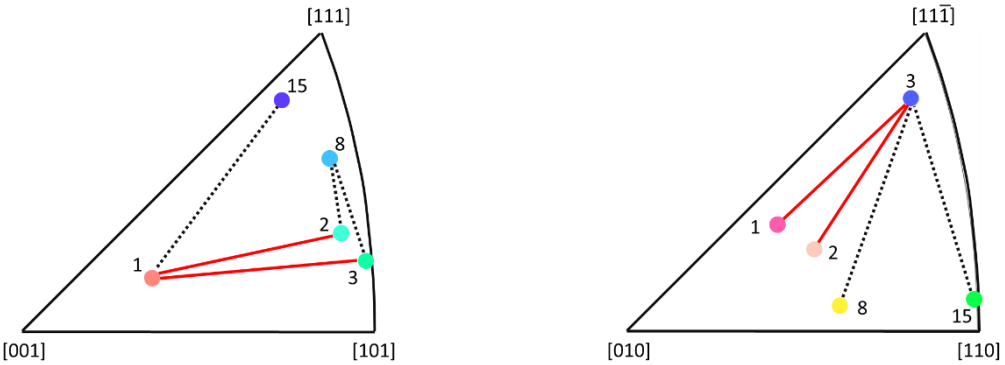

Figure 6-11: Orientation of cracked (red) and uncracked (black dotted) grains in IPF-pole figure; left: Orientation in loading direction (x), right: Orientation in horizontal direction (y).

Critical parameters for crack initiation due to grain orientation differences

Grain size and grain boundary alignment were identified as important geometric parameters for creep (fatigue) crack initiation. Large grains are more susceptible to crack initiation. Depending on mechanism, grain boundary sliding can occur in directions of maximum resolved shear stress. Horizontal grain boundaries are prone to crack initiation under high normal stresses. With regard to the grain orientations, it can be concluded that [101]-oriented grains were often found near secondary cracks. These grains show a strongly anisotropic elastic behaviour. Using the Schmid factors, a prediction of creep behaviour is possible where a large difference of maximum Schmid factors could be identified as critical. The

crystal plasticity simulations have shown that grains with unfavourable orientations (close to the [025] direction in loading direction) are susceptible to large inelastic strains which could be critical for crack initiation in adjacent grain boundaries, in particular if neighbouring grains have crystal orientations (close to the [101] or [111] direction) that show small tendency for creep. Moreover, if cracks initiate before inelastic strains can develop, stress field concentrations due to high misorientations of neighbouring grains could be critical for crack initiation.

7 Validation

The validation of the elastic and inelastic microstructure-based FE models with regard to the deformation behaviour was carried out using optical strain field measurement by utilizing the stereo camera system Aramis (GOM). For this purpose, an experimental approach was developed fulfilling several requirements. Furthermore, a goal was to examine whether a critical grain orientation combination could be verified and a prediction of the crack initiation spot is possible.

7.1 Experimental approach

A flat specimen with a thickness of 2 mm was chosen so that a more or less constant microstructure in the depth direction could be assumed for the given grain size. (Figure 7-1). Since no non-destructive testing method exists capable of capturing the 3D microstructure, the EBSD measurement was performed on the counterpart of both specimen surfaces. The back side was checked via EBSD to verify the assumption made. A certain agreement with the front side was found, but it became clear that a nearly directionally solidified (DS) microstructure does not apply. The grain boundaries lie at an arbitrary angle in depth direction but the number of additional grains on the back side was low.

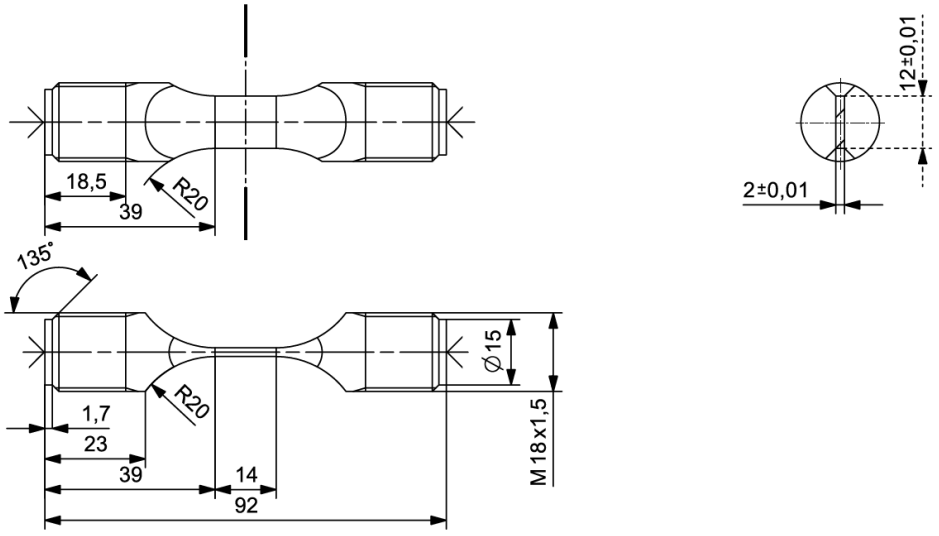

Figure 7-1: Specimen geometry for validation tests.

In order to be able to capture the specimen surface with the camera system, an induction heating device was chosen and an optimized coil design, mounted on the back side only, has been developed. The temperature distribution was measured with a thermal imaging camera (Figure 7-2). In transvers direction, the temperature shows a homogeneous distribution with a deviation of +/- 5 °C. In longitudinal direction, the temperature distribution reveals as sufficient in order to reliably perform the validation test series.

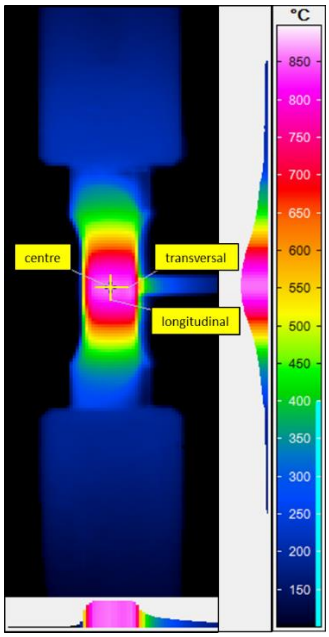

ID	avg. (°C)	min (°C)	max (°C)	length (mm)
centre	855	-	-	-
transversal	852	848	858	11
longitudinal	843	827	855	8

Figure 7-2: Temperature distribution for the validation tests measured by a thermal imaging camera.

7.2 Results

For the specimens of the validation tests, the EBSD measurement was performed on the counterpart of the specimens and afterwards the FE models were created, as described in chapter 6.1. The first test was performed at 850 °C with a net stress of 300 MPa (Figure 7-3).

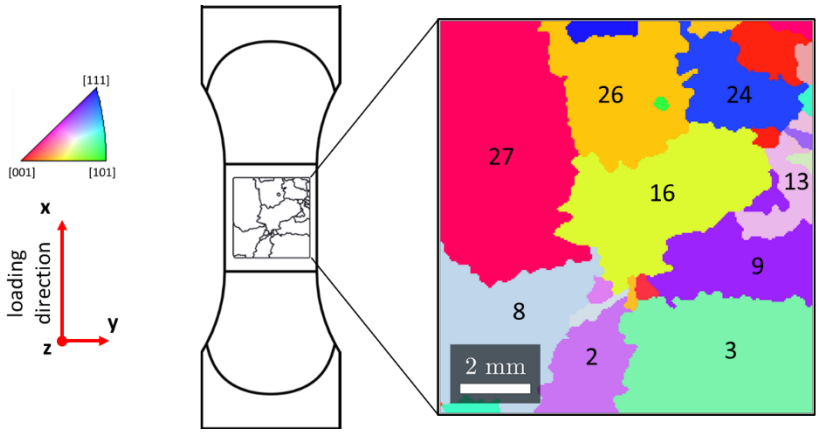

Figure 7-3: First validation test specimen and EBSD measurement, Orientation plotted in x-direction.

For the anisotropic linear-elastic model, the measured elastic constants C_{11}, C_{12} and C_{44} were used for defining the orthotropic material behaviour. The measured strain distribution from the camera system after loading shows a very good agreement with the calculated elastic strain distribution (Figure 7-4). The highest local strains occur in grain 26 and grain 27 as could be expected for grain orientations near [001]. Since the elastic model considers the grain boundaries as boundaries of elastic moduli, the strain distribution is sharply contoured. In the optical measurement, this sharp separation does not show up at all grain boundaries as expected.

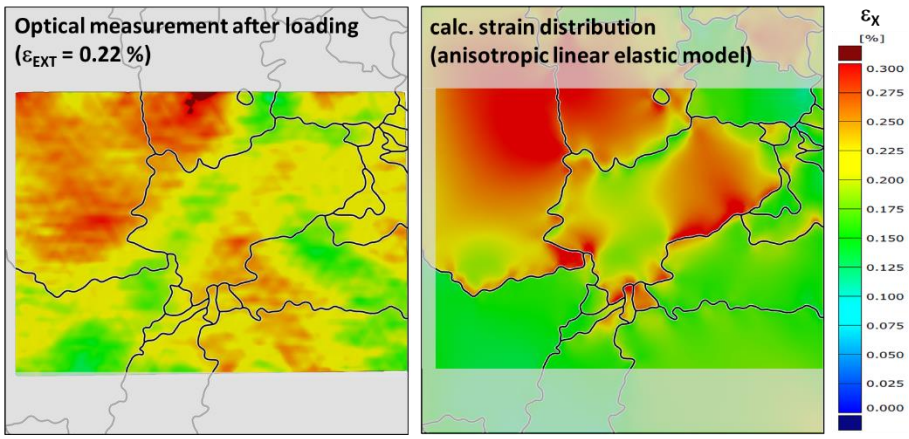

Figure 7-4: Comparison of measured (GOM) and calculated (anisotropic elastic) strain distribution in loading direction (x) after loading the specimen.

For the comparison of the global creep strain, a virtual extensometer was placed in both the Aramis system and the now viscoplasticity-activated FE model, Figure 7-5. The calculated creep strain at the extensometer position shows an overall good agreement in the secondary creep regime up to a duration of 200 h, Figure 7-5. Please note again, that tertiary creep is not considered in the creep model. It is noticeable that in the primary creep regime the calculated creep strain is lower than the one from the optical measurement. Additionally, local strains in selected grains were evaluated (Figure 7-5). During the first hours of the creep test, it can be seen that the primary creep strain measured in grain 27 at the marked spot is about 30% higher than in the other grains. This trend continues almost throughout the entire test duration. In the secondary creep regime, a higher local creep strain is measured also within grain 9.

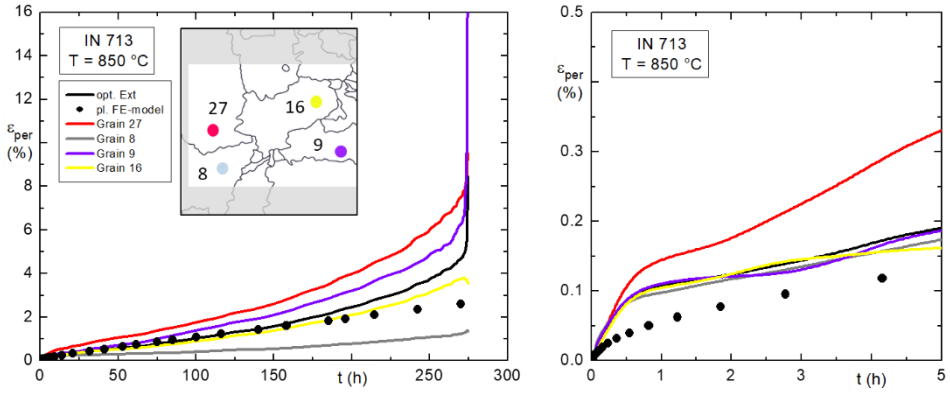

Figure 7-5: Comparison of the measured and calculate creep strain from the first validation test.

The comparison of the calculated and measured local creep strain distribution in the secondary creep regime is shown in Figure 7-6. The creep simulations lead to local maxima of creep strain in grains 16, 26 and 27 which have an orientation close to [025] in loading direction. In the optical measurement, a slightly different strain distribution with maxima only in grains 26 and 27 was found. The reason for this discrepancy could be that the variation of the grain structure perpendicular to the sample surface was not taken into account in the simulations.

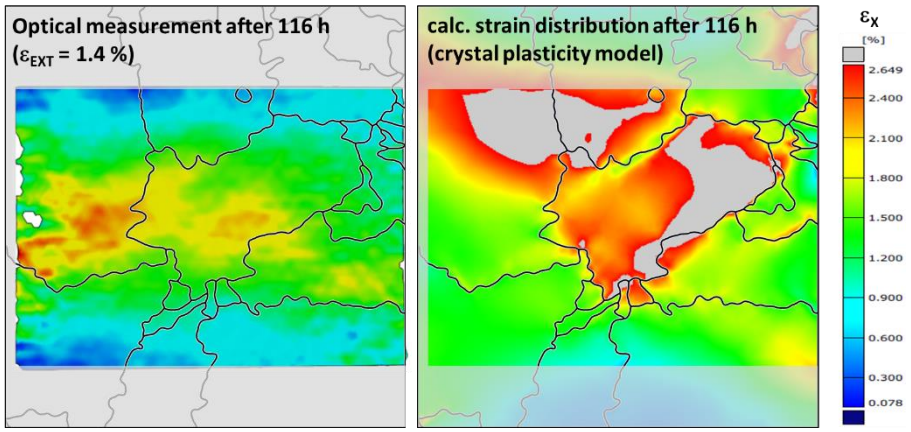

Figure 7-6: Comparison of measured (GOM) and calculated (crystal plasticity) strain distribution in loading direction (x) after 116 h.

Based on the microstructure and the evaluated potential critical parameters, a prediction was made which grain boundaries are preferred for crack initiation (Figure 7-7). Due to geometrical reasons, there were five possible grain boundaries that could be considered for creep crack damage. Grain 3 is the only grain with a critical [101] orientation and strong anisotropic Poisson ratio. Additionally, the {111}<121> slip system is highly stressed due to a maximum Schmid factor of 0.493 and the calculated stress from the linear-elastic model. The difference of the max. Schmid factor to grain 9 is maximum with a value of 0.1 and the misorientation angle between both is 41°. The difference of the maximum Schmid factor for secondary creep slip system {111}<101> is 0.8. Based on the parameters mentioned above, this grain boundary between grain 3 and grain 9 was determined as critical before the test was conducted.

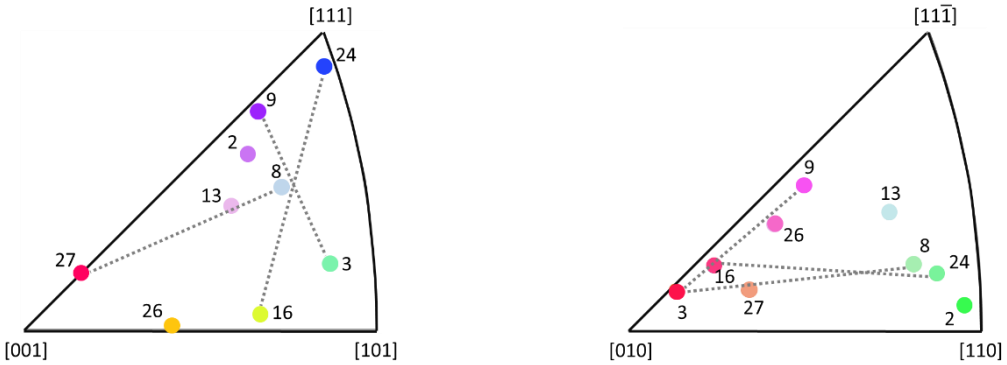

Figure 7-7: Critical grain orientation combinations, left: Orientations in loading direction (x), right: Orientations horizontal to loading direction (y).

Besides that, two other grain combinations (8 | 27 and 16 | 24) seemed to be critical from the calculated strain distribution in loading direction. From the differences in measured creep strain, there is a very good agreement of the maximum Schmid factor for primary creep of 0.5 in grain 27 and the high local amount of primary creep strain. Furthermore, the misorientation angle of grain 8 and grain 27 is about 54°. The misorientation angle at the boundary between grain 16 and 24 is only 34°, but the differences in the maximum Schmid factor for the octahedral system is 0.165. According to theory, there should be a clear difference with regard to secondary creep. Nevertheless, this could not be verified from the optical strain measurement.

The specimen was broken during the first validation test so that the crack initiation site could not be identified. However, the crack path could be compared with the predicted critical grain boundaries. The cracked grain boundaries between grains 8 | 27 and 3 | 9 were two of them, but they are also the longest available horizontal grain boundaries. Based on this result, no clear conclusion could be made regarding a critical grain orientation combination.

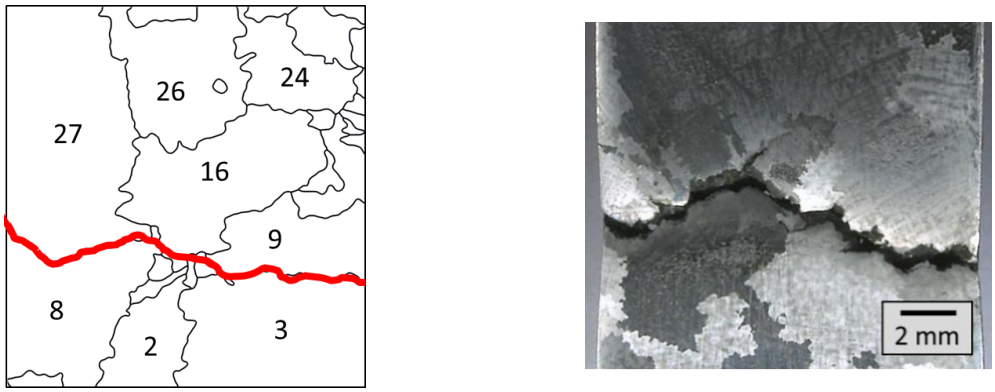

Figure 7-8: First validation specimen broken in the test along grain 8 | 27 and 3 | 9, left: Grain structure with cracked grain boundaries (red), right: Etched microstructure of the broken specimen.

The second validation test was performed with the same parameters (850 °C, 300 MPa) in order to stop the test in time so that a critical orientation for the crack initiation could be identified. This specimen shows a strong deviation of the orientation distribution compared to the first specimen. The orientation in loading direction shows an aggregation of grains with an approximate orientation of [101] (Figure 7-9). Especially grain 9, grain 10 and grain 13 show a slight deviation from this orientation.

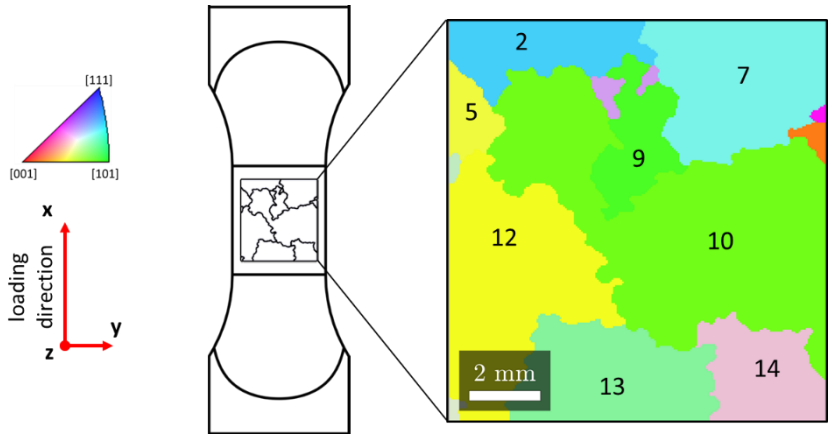

Figure 7-9: Second validation specimen and EBSD measurement, Orientation plotted in x-direction.

This test was stopped after 42 h to prevent the failure of the specimen. From the optical strain measurement, it can be seen that the tertiary creep regime was reached (Figure 7-10) and a creep crack was visible on the surface (Figure 7-11). The first validation test with the same parameters was finished after 272 h. This difference in lifetime can be explained by the different grain orientations. As reported in [Mac82], creep rupture lives for [101]-oriented single crystals are extremely poor (Figure 2-3). Due to the large grain size of grain 10 with the mentioned orientation of [101], a significant influence on the creep behaviour of the polycrystal can be assumed. Additionally, grain 12 has an orientation of about [025], which was identified as an unfavourable orientation, and therefore high creep strains were expected. These conclusions lead to an opposite creep behaviour of these two grains.

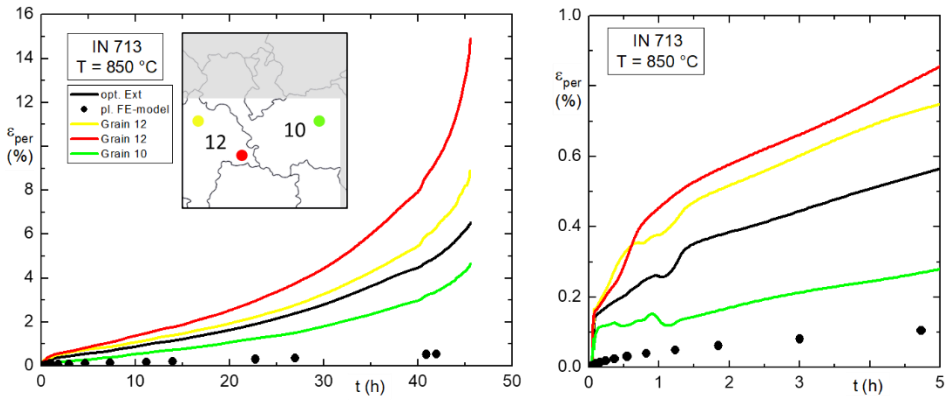

Figure 7-10: Comparison of the measured and calculate creep strain from the second validation test.

Calculating the Schmid factors for both possible slip systems, the theory of primary creep on the {111}<112> system could not be verified. The highest creep strain was measured in grain 12 and correlates with the maximum Schmid factor for the octahedral slip system and the prediction from the crystal plasticity model. The creep crack occurred at the grain boundary between grain 12 and 13, which has a high misorientation angle of about 56°. Although more horizontal grain boundaries are present, no further creep damage could be detected. Therefore, in this case, the orientation combination of [025] and [101] can be identified as critical.

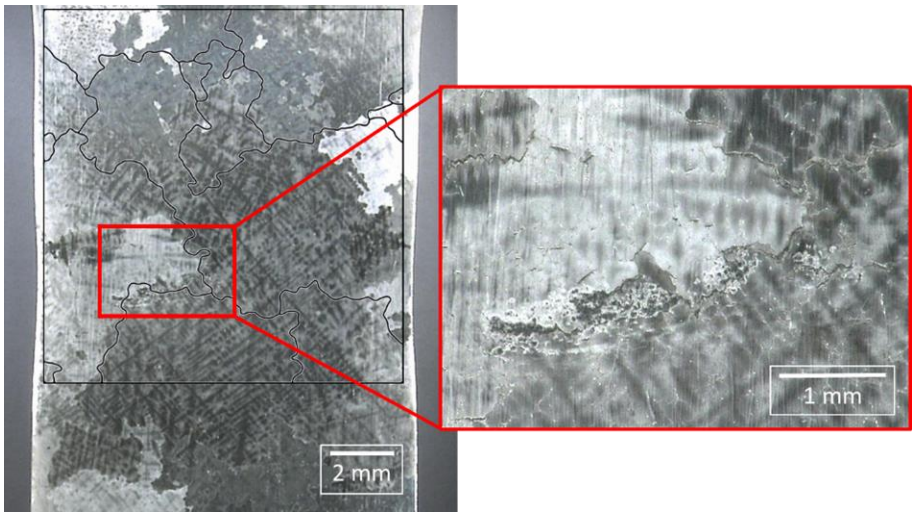

Figure 7-11: Etched specimen from the second validation test with visible creep crack between grain 12 and 13.

8 Summary and conclusions

The objective of this research project was to establish an improved description of the crack behaviour of coarse-grained nickel cast alloys under creep and creep-fatigue loading. In order to achieve this goal, a comprehensive work program was defined. This includes tests for the material model parameter identification on three different IN713 alloys (polycrystal as well as single crystals with two different orientations [001] and [121]) and crack propagation tests under creep (fatigue) loading on a polycrystalline alloy IN713 CC at 850 °C including validation tests. Furthermore, accompanying extensive metallographic and electron microscopic examinations were carried out.

The findings from the experimental part have been implemented in numerical simulations. A procedure was developed to transfer EBSD data in a quasi 3D microstructural model. The modelling of the material

behaviour was done with an anisotropic linear-elastic model and a more complex crystal plasticity model (Cailletaud). These models were validated using the results from validation tests which were accompanied by local strain measurements. Differences between the models and experimental results can be attributed to the unknown extension of the microstructure in depth direction. In the primary creep regime, large local strain differences depending on the grain orientations were measured. Hence, the crystal plasticity model should be extended accordingly. Further investigations should be done if the use of {111}<112> slip systems for modelling primary creep is suitable.

Afterwards, the focus was on the development of critical parameters to asses a “grain orientation mismatch induced crack initiation” under creep (fatigue) loading. The findings in this regard can be summarized as follows:

- The occurrence of high local strains could be correlated with maximum Schmid factors of the octahedral slip system.
- The differences of the maximum Schmid factors of the octahedral slip system and high misorientation angles were evaluated as critical for creep crack initiation.
- A critical grain orientation combination of [101] and [025] for the crack formation were determined using a crystal plasticity model and could be verified based on the results of the validation tests.
- Geometric parameters are significant for creep crack initiation and growth, and therefore the influence of the microstructure in depth direction should be part of further research.

In order to verify the results, it is necessary to further improve the understanding of relevant mechanisms, possibly by in-situ experiments.

9 Appendix

Bibliography

[AMS14] AMS 5391: Nickel Alloy, Corrosion and Heat-Resistant, Investment Castings 73Ni-0.14C-4.5Mo-2.3Cb(Nb)-0.75Ti-6.0Al-0.010B-0.12Zr Vacuum Cast, As-Cast; Sae International: Warrendale, PA, USA, 2014.

[Bac11] Bachmann, F., R. Hielscher, H. Schaeben: Grain detection from 2d and 3d EBSD data – Specification of the MTEX algorithm, Ultramicroscopy 111, 2011, 1720-1733.

[Ben03] Bennett, V.P., D.L. McDowell: Polycrystal orientation distribution effects on microslip in high cycle fatigue, Int. J. Fatigue 25 (2003) 27-39.

[Ber03] Berger, C. et al.: Rissverhalten von Nickelbasislegierungen unter überlagerter Kriech- und Ermüdungsbeanspruchung: FVV Final report of AiF project 12308 N, IfW TU Darmstadt, MPA Universität Stuttgart, 2003.

[Ber08] Berger, C. et al.: Absicherung von Konzepten zur Beschreibung des Rissverhaltens der Legierungen Inconel 706, Inconel 718 und IN-738 LC unter überlagerter Beanspruchung: FVV Final report of AiF project 14609N, IfW Darmstadt, TU Darmstadt, Materialprüfungsanstalt Universität Stuttgart, 2008.

[Ber10] Berger, C. et al.: Rissverhalten von Nickelbasis-Gusslegierungen mit unterschiedlicher Korn-struktur: FVV Final report of AiF project 15626N, IfW Darmstadt, TU Darmstadt, Materialprüfungsanstalt Universität Stuttgart, 2010.

[Bot97] Bothe, K., K. Kußmaul, K. Kollmann: Langzeitfestigkeitsverhalten bei Temperaturen im Kriechgebiet – Untersuchung des Zusammenhanges von Zeitstandeigenschaften und Auswirkungen überlagerter Dehnungswechselbeanspruchung. Final report, AiF-Nr. 9348, Staatliche Materialprüfungsanstalt Universität Stuttgart, 1997.

[Bra95] Branco, C.M., R. Ritchie, V. Sklenicka: Mechanical Behaviour of Materials at High Temperature, Proceedings of the NATO Advanced Study Institute on Mechanical Behaviour of Materials at High Temperature, Sesimbra, Portugal, September 12-22, 1995, 93-134.

[Che07] Cheong, K.S., M.J. Smillie, D.M. Knowles: Predicting fatigue crack initiation through image-based micromechanical modeling Acta Mater. 55 (2007) 1757–1768.

[Cor04] Lückemeyer, N., M. Reigl, M. Schwienheer, A. Udoh: BMWI-PTJ-Verbundvorhaben COORETEC-turbo 4.1.1A (COORETEC DT4), Lebensdauerkonzepte und bruchmechanische Bewertung für Hochtemperaturdampfturbinen bis 720 °C, Final report, 2011.

[Dem71] Demarest, H.: Cube resonance method to determine the elastic constants of solids. J Acoust Soc Am, 49, 1971, 768–775.

[Dep19] Depriester, D.: MTEX2Gmsh, DOI: 10.5281/zenodo.2595052, https://github.com/Dorian-Depriester/mtex2Gmsh (31.10.2019).

[Dun07] Dunne, F.P.E, A.J. Wilkinson, R. Allen: Experimental and computational studies of low cycle fatigue crack nucleation in a polycrystalInt. J. Plast. 23 (2007) 273–295.

[Eng18] Engel, B. et al.: Effect of local anisotropy on fatigue crack initiation in a coarse grained nickel-base superalloy, MATEC Web Conf. 165, 2018, 04004.

[Gui10] Guilhem, Y., S. Basseville, F. Curtit, J.-M. Stéphan, G. Cailletaud: Investigation of the effect of grain clusters on fatigue crack initiation in polycrystals, Int. J. Fatigue 32 (2010) 1748-1763.

[Har99] Harder, J.: A crystallographic model for the study of local deformation processes in polycrystals, Int. J. Plast. 15 (1999) 605-624.

[Hei90] Heinz, A., P. Neumann: Crack Initiation During High Cycle Fatigue of an Austenitic Steel, Acta Metallurgica et Materialia, 38, 1990, 1933.

[Kir18] Kirmaier, F.: Simulation von Spannungsüberhöhungen an Korngrenzen infolge von Kornorientierungsunterschieden, TU Darmstadt, Bachelor Thesis, 2018.

[Kno01] Knowles, D.M., S. Gunturi: The role of <112>{111} slip in the asymmetric nature of creep of single crystal superalloy CMSX-4, Materials Science and Engineering: A 328, 2002, 223-237

[Kno05] Knorr, S.: Development and Application of Grain Scale FE-Models for Polysilicon based on EBSD Mappings, HTWK Leipzig, Diplomarbeit, 2005.

[Kru02] Krupp, U. et al.: Mechanisms of Short-Fatigue-Crack Initiation and Propagation in a ß-Ti Alloy, Philosophical Magazine A, 82, 2002, 3321.

[Lat16] Latypov, M. I. et al.: Micromechanical finite element analysis of strain partitioning in multiphase medium manganese TWIP+TRIP steel, Acta Materialia 108, 2016, 219-228.

[Li15] Li, Z., et al.: Deformation and recrystallization of single crystal nickel-based superalloys during investment casting, Journal of Materials Processing Technology, 217, 2015, 1-12.

[Lin10] Lin, B., L.G. Zhao, J. Tong, H.-J. Christ: Crystal plasticity modeling of cyclic deformation for a polycrystalline nickel-based superalloy at high temperature, Mater. Sci. Eng. A 527, 2010, 3581-3587.

[Mac82] MacKay, R.A., R.D. Maier: The influence of orientation on the stress rupture properties of nickel-base superalloy single crystals. Metall Mater Trans A 13, 1982, 1747–1754.

[Mer91-1] Meric, L., P. Poubanne, G. Cailletaud: Single Crystal Modeling for Structural Calculations: Part 1 – Model Presentation. ASME Journal of Applied Mechanics 113, 1991, 162-170.

[Mer91-2] Meric, L., G. Cailletaud: Single Crystal Modeling of Structural Calculations: Part 2-Finite Element Implementation. ASME Journal of Applied Mechanics 113, 1991, 171-182.

[Naz83] Nazmy, M.Y., C. Wüthrich: Creep crack growth in IN-738 and IN-939 nickel-base superalloys, Materials Science and Engineering 61, 1983, 119-125.

[Oec11] Oechsner, M., L. Serrano, Schweizer C, A. Scholz, F. Mueller, C. Berger et al.: Rissverhalten unter anisothermen Beanspruchungsbedingungen – Berechnungsverfahren für Nickelbasislegierungen: Final report of AiFproject 15525 N, 2011.

[Oec14] Oechsner, M., K. Maile, A. Scholz, A. Klenk, Ch. Baumann, M. Speicher, F. Müller, Ch. Kohler: Bewertung des Rissverhaltens von Fehlstellen hochtemperaturbeanspruchter Schaufeln aus Nickelbasisgusslegierungen, Final report of AiF project 17195 N, IfW TU Darmstadt, MPA Universität Stuttgart, 2014.

[Oec17] Oechsner, M., K. M. Krämer, C. Schweizer, A. Scholz, F. Mueller et al.: Zeitabhängiges Rissverhalten unter anisothermen Beanspruchungen - Entwicklung und Validierung von Berechnungsmethoden: Final report of AiFproject 17809 N, 2017.

[Ohn76] Ohno, I.: Free vibration of a rectangular parallelepiped crystal and its application to determination of elastic constants of orthorhombic crystals, Journal of Physics of the Earth, 24 (4), 1976, 355-379.

[Pan97] Pan L. M., B.A. Shollock, M. McLean: Modelling of high-temperature mechanical behaviour of a single crystal superalloy, Proc. R. Soc. Lond. A. 453, 1997, 1689–1715.

[Per94] Peralta, P., L. Llanes, J. Bassani, C. Laird: Deformation from Twin-Boundary Stresses and the Role of Texture: Application to Fatigue, Philosophical Magazine A, 70, 1994, 219.

[Pfe17] Pfeiffer, S., M.F.-X. Wagner: Elastic deformation of twinned microstructures, Proc. R. Soc. A 473: 20170330, 2017.

[Pol06] Pollock, T. M., S. Tin: Nickel-Based Superalloys for Advanced Turbine Engines: Chemistry, Microstructure and Properties, J. of Propulsion and Power 22 (2), 2006, 361-374.

[Sas96] Sass, V., U. Glatzel, F.-K. Monika: Creep Anisotropy in the Monocrystalline Nickel-Base Superalloy CMSX-4, Superalloys 1996, Warrendale, Pa., 1996, 283-290.

[Sha89] Shahinia, P., K. Sadananda: Creep and fatigue crack growth behaviour of some cast nickel-base alloys, Materials Science and Engineering 108, 1989, 131-140.

[She08] Shenoy, M., Y. Tjiptowidjojo, D. McDowell: Microstructure-sensitive modelling of polycrystalline IN 100, Int. J. Plast. 24, 2008, 1694–1730.

[Sie01] Siebörger, D., H. Knake, U. Glatzel: Temperature dependence of the elastic moduli of the nickel-base superalloy CMSX-4 and its isolated phases, Materials Science and Engineering: A 298, 2001, 26-33.

[Sou08] Soula, A., et al., Grain boundary and intragranular deformations during high temperature creep of PM Ni-based superalloys, in Superalloys 2008, 2008, 387-93.

[Sti15] Stinville, J.C., K. Gallup, T.M. Pollock: Transverse Creep of Nickel-Base Superalloy Bicrystals, Metall Mater Trans A 46, 2015, 2516–2529.

[Sun13] Sun, J.: Time-dependent crack growth in a coarse-grained Ni-based superalloy RR1000, Ph.D. thesis, University of Birmingham, 2013.

[Swa13] Swaminathan, K., J. Blendell, K. Trumble: Effect of crystallographic orientation on subcritical grain boundary cracking in a conventionally cast polycrystalline nickel-based superalloy, Microscopy and microanalysis: the official journal of Microscopy Society of America, Microbeam Analysis Society, Microscopical Society of Canada, 19 (4), 2013, 978-87.

[Tin10] Tinga, T., W.A.M. Brekelmans, M.G.D. Geers: Cube slip and non-Schmid effects in single crystal Ni-base superalloys, Modelling and simulation in materials science and engineering, 18(1), 2010, 015005.

[Wol19] Wöllmann, L., F. Mueller, M. Speicher, C. Kontermann, M. Oechsner: Einfluss der elastischen Anisotropie auf das Kriechrissverhalten grobkörniger Nickelbasislegierungen, 42. Vortragsveranstaltung „Langzeitverhalten warmfester Stähle und Hochtemperaturwerkstoffe, Düsseldorf, 2019.